https://doi.org/10.5194/se-2021-75
Preprint. Discussion started: 14 June 2021

Solid Earth
Discussions
Open Access
EGU

GPR signature of Quaternary faulting: a study from the Mt. Pollino region, southern Apennines, Italy.

Maurizio Ercoli[1-4], Daniele Cirillo[2-4], Cristina Pauselli[1-4], Harry M. Jol[3], Francesco Brozzetti[2-4]

[1]: Università degli Studi di Perugia, Dipartimento di Fisica e Geologia, Piazza dell'Università 1, 06123 Perugia, Italy.
[2]: Universita "G. d'Annunzio" di Chieti-Pescara, DiSPUTer, via dei Vestini 31, 66100 Chieti, Italy.
[3]: University of Wisconsin - Eau Claire, Department of Geography and Anthropology, 105 Garfield Avenue, Eau Claire, WI, 54702.
[4]: CRUST Centro inteRUniversitario per l'analisi SismoTettonica tridimensionale, Italy.

Correspondence to: Maurizio Ercoli (maurizio.ercoli@unipg.it; maurizio.ercoli@gmail.com)

Abstract. With the aim of unveiling evidence of Late Quaternary faulting, a series of Ground Penetrating Radar (GPR) profiles were acquired across the Campotenese continental basin (Mt. Pollino region) in the southern Apennines active extensional belt (Italy). A set of forty-nine 300 MHz and 500 MHz GPR profiles, traced nearly perpendicular to a buried normal fault, were acquired and carefully processed through a customized workflow. The data interpretation allowed us to reconstruct a pseudo-3D model depicting the boundary between the Mesozoic bedrock and the sedimentary fill of the basin, which were in close proximity to the fault. Once reviewing and defining the GPR signature of faulting, we highlight ~~in our data how~~ near surface alluvial and colluvial sediments ~~appear to be~~ dislocated by a set of conjugate (west and east-dipping) discontinuities that penetrate inside the underlying Triassic dolostones. Close to the contact between the continental deposits and the bedrock, some buried scarps which offset wedge-shaped deposits are interpreted as coseismic ruptures, subsequently sealed by later deposits. Although the use of pseudo-3D GPR data implies more complexity linking the geophysical features among the radar images, we have reconstructed a reliable subsurface fault pattern, discriminating master faults and a series of secondary splays. We believe our contribution provides an improvement in the characterization of active faults in the study area which falls within the Pollino seismic gap and is considered potentially prone to severe surface faulting. Our aim is for our approach and workflow to be of inspiration for further studies in the region as well as for similar high seismic hazard areas characterized by scarcity of near-surface data.

Key-words: *Ground Penetrating Radar (GPR); Image processing; Faults; Neotectonics; Palaeoseismology; Earthquake hazards.*

1. Introduction

A *"seismic gap"* is a region characterized by active faults that are seismically "*silent*" during the historical record (~~Galadini and Galli 2003~~), ~~but which are considered,~~ on the basis of paleoseismological and/or morpho-structural data, able to generate significant earthquakes (McCann et al. 1979; Mogi 1979; Plafker and Galloway 1989). Although the hypothesis stating that the earthquake potential increases after a long quiet period was rejected by some authors (Kagan and Jackson 1991), in some cases fault segments located in areas of longstanding gaps have revealed their seismic potential, by producing earthquakes of moderate or high magnitude. Late Quaternary activity related to normal faults can be suggested by structural and geomorphological evidence, as happens also in many sectors of the active Italian

https://doi.org/10.5194/se-2021-75
Preprint. Discussion started: 14 June 2021

extensional province, but their seismogenic role of such faults is not well understood yet. As shown by the 2016-2017 seismic sequence in central Apennines (Chiaraluce et al. 2017; Galli et al. 2019), the Italian Apennines can be considered an ideal laboratory for all geoscience disciplines studying seismic gaps. This seismic crisis occurred in an area displaced by an alignment of west-dipping Quaternary faults, where no important earthquakes had been recorded over the past 1500 years. Nine-strong and moderate seismic events struck a ~80 km long region, climaxing in the Mw = 6.5 "Norcia" mainshock (Porreca et al. 2018 and references therein; Ercoli et al. 2020), producing extensive surface faulting (Pucci et al. 2017; Civico et al. 2018; Villani et al. 2018; Brozzetti et al. 2019, 2020; Testa et al. 2019; Cirillo 2020). Geological and paleoseismological studies across the faults set were preceding this seismic sequence (Calamita et al. 1992; Brozzetti and Lavecchia 1994; Barchi et al. 2000; Galadini and Galli 2003, Galli et al. 2008). Besides, some years before this sequence, 2D/3D GPR surveys (Ercoli et al. 2013a; 2014) detected a peculiar geophysical signature confirming buried past surface faulting in Holocene deposits, that was not very prominent on the present topography. These studies revealed occurrence of strong paleo-earthquakes and led to consider the Mt. Vettore master fault "silent", but prone to cause similar strong events in the future. This proves the paleoseismological approach can be of great help in many tectonically active areas of the Apennines. Its systematic application may provide answers on both the seismic potential and the recurrence times (Mc Calpin; Galli at al. 2008; 2019; 2020). But on many active faults, contrary to geophysical surveys, paleoseismological data cannot be carried out systematically due complex logistics, environmental restrictions, the relatively high costs and, authorization processes. In addition, in many terrestrial areas, past coseismic ruptures can be poorly visible at surface, as undergoing to natural or/and anthropogenic topographic "regularization". Thus, when also other geological, seismological, and geophysical data are scarce, outdated, or not detailed enough for the definition of a satisfactory seismotectonic framework, Quaternary silent faults in "*seismic gaps*" deserve great attention for local seismic hazard evaluation. For the above reasons, Quaternary faults and associated basins have been and are currently investigated not only Central Italy, but also in the southernmost Apennines sector (Galli et al. 2008; 2020). A dedicated research project (Agreement INGV-DPC 2012-2013 and 2014-2015, Project S1 - Base-knowledge improvement for assessing the seismogenic potential of Italy, Brozzetti et al. 2015; Pauselli et al. 2015) aiming to improve the base-knowledge of seismogenic structures was focused during the 2012-2015 period also on the Calabrian region (Southern Italy).

In the project, structural geological, geophysical, and paleoseismological studies were successfully acquired across the Mt. Pollino and Castrovillari fault systems (northern Calabria), supporting evidence of their Late Quaternary activity (Ercoli et al. 2013b; Cinti et al. 2015, Ercoli et al. 2015; Brozzetti et al., 2017b). This area, which is considered one of the most important seismic gaps in southern Italy, extends northward to include the Mercure and Campotenese basins, both characterized by Late Quaternary continental syn-tectonic sedimentation (Fig. 1a-c).

The fresh geomorphic signature of the faults bounding these basins suggests Late Quaternary activity; besides, paleoseismological trenching and radiocarbon dating document the occurrence of $M_w > 6.5$ paleo-earthquakes (Cinti et al. 1997, 2002; Michetti et al. 1997, 2000). But the data contrasts with the poor historical seismicity, reporting a single significant $M_w = 5.6$ event occurred in 1693 (Guidoboni et al. 2018) and, ultimately, also with instrumental seismicity characterized by two moderate seismic sequences respectively climaxed in the Mw 5.6 Mercure (1998, September 9) and Mw 5.2 Mormanno (2012, October 25) earthquakes. The latter occurred during a long-lasting sequence spanning the period 2010-2014, which included more than 6000 seismic events of $M_w > 1$ and activated at least three individual seismogenic sources (Passarelli et al., 2015; Brozzetti et al., 2017a; Cirillo et al., 2021; Fig. 1b). The gap between the low energy release, observed during the instrumented seismic sequences, and the high seismic potential estimated for the Quaternary faults, raised the question of whether even stronger earthquakes had shaken and

https://doi.org/10.5194/se-2021-75
Preprint. Discussion started: 14 June 2021

could shake the area in the future. A recent and detailed parameterization of the Fosso della Valle-Campotenese fault (VCT), that bounds a homonym basin (Fig. 1c) showing both geological and seismological evidence of current activity (Totaro et al. 2014, 2015; Brozzetti et al. 2017a, ~~Cirillo et., 2021~~), assesses a surface length of ~15 km and a depth of at least 10 km (Brozzetti et al. 2017a; Cirillo et al., 2021): the potential rupture-area is likely estimated to produce M_w > 6.0 earthquakes. ~~Such seismic events,~~ in the Apennines extensional belt, ~~are~~ generally ~~considered capable of~~ producing ~~coseismic~~ surface ~~breaks~~ (Pantosti and Valenzise 1990; ~~Cello et al. 2000~~; ~~Vittori et al. 2000~~; Boncio et al. 2010; Villani et al. 2018; Brozzetti et al. 2019). However, evidence of Quaternary faulting for this structure is currently unclear, but geological and morpho-structural data suggest this fault has played an important role in determining the geometry and the recent sedimentary evolution of the basin.

The Campotenese basin and its VCT boundary fault is an emblematic example that summarizes the aforementioned issues: 1) unavailability of paleoseismological data as the basin is entirely located within the Mt. Pollino National Park, thus requiring prior authorization from competent authorities; 2) unavailability of publically geophysical data; 3) no fresh surface displacements of Holocene deposits, suggesting the occurrence of recent strong earthquakes, have been observed so far along its trace.

For all these reasons, the VCT represents an ideal case study suitable to test our working method, as ~~it~~ we have conducted an explorative GPR campaign as a screening tool for the ~~detections of potential unknown Quaternary co-seismic ruptures along its fault zone~~. It is possible that, during past strong earthquakes, propagation of coseismic ruptures along the fault could have displaced Holocene deposits at the surface, being subsequently buried by further and more recent alluvial deposits or erased by the anthropogenic and agricultural activity. The objectives of the project are to: i) review and describe geophysical characteristics associated with a peculiar GPR signature of faulting, and propose a methodological GPR workflow for the study site which might be extended to other areas; ii) check the efficiency of a GPR prospection in the Campotenese study site to locate the trace of the studied fault as well as verifying its spatial continuity at depth; iii) provide new data to relate ~~to~~ the occurrence of M_w > 6.0 events on the VCT~~, as observed for the nearby Castrovillari faults;~~ iv) highlight new elements for more exhaustive characterization of the VCT with the purpose of better quantifying its seismogenic potential; v) pave the way for other local geophysical prospections and identify interesting sites for future ground-truthing and/or paleoseismological trenching; vi) to have direct application and impact to the planning of future mitigation strategies for the reduction of surface faulting risk in the nearby urbanized areas.

2. Tectonic setting and seismicity

The Campotenese continental basin is located in the northernmost Calabria region south-west of the Mt. Pollino calcareous massif (southern Italy, Fig. 1). The bedrock of the basin consists of shallow water dolostones and limestones, Late Triassic to Middle Miocene in age, belonging to the Verbicaro tectonic unit (Ogniben 1969; Amodio Morelli et al. 1976). It is generally referred to the western edge of the "Apenninic Platform", a thick (>4 km) carbonate shelf, that underwent compression during the Middle-Late Miocene times and was translated over an eastern basinal domain (Lagronegro-Molise basin; Patacca and Scandone 2007; Vezzani et al. 2010 and references therein). From the bottom to the top, the bedrock succession includes late Triassic dolostones, Cretaceous limestones, and Paleocenic-Lower Miocenic calcarenites cross-cut by the pillow lava basalts belonging to Liguride units of the northern sector of Calabrian arc (Quitzow 1935, Grandjaquet and Grandjaquet 1962, Amodio Morelli et al. 1976, Ghisetti and Vezzani, 1983; Iannace et al. 2004, 2005 and 2007; Liberi et al. 2006; Filice et al. 2015 and Tangari et al. 2018).

https://doi.org/10.5194/se-2021-75
Preprint. Discussion started: 14 June 2021


Solid Earth
Discussions
Open Access
EGU

The origin of the Campotenese basin, however, is related to a set of NW-SE striking extensional faults which, during the Middle-Late Pleistocene, displaced the contractional tectonic pile, favoring the deposition of alluvial and lacustrine sediments in a subsiding intra-mountain depression (Servizio Geologico d'Italia 1970). This set of conjugate SW- and NE-dipping normal faults represents the local expression of the Quaternary extensional belt that develops all along the Italian peninsula, nearly parallel to the axial zone of the Apennines, from northern Tuscany to the Calabrian Arc (Brozzetti 2011). North of Campotenese, (Lucania and southern Campania) the Apennine extensional belt includes several continental basins and their boundary faults, as the Irpinia, Vallo di Diano, Tanagro, Melandro-Pergola and Val d'Agri (Ascione et al. 1992; Maschio et al. 2005; Amicucci et al. 2008; Villani and Pierdominici 2010; Brozzetti 2011; Filice and Seeber 2019 and Bello et al. 2021). To the south, it continues with the Crati graben that dissects the northern sector of the Calabrian Arc (Tortorici et al. 1995; Brozzetti et al. 2017b).

On the regional scale, the Quaternary normal fault array controls the release of major seismicity, as suggested by the distribution of supra-crustal instrumental earthquakes (INGV 2020 and Iside 2007) and of the strongest historical events (Fig. 1a, Tertulliani and Cucci 2014; Rovida et al. 2020). Several seismological and paleo-seismological investigations claim that most of the faults bounding the Quaternary basins are seismogenic and therefore enable, in some cases, to associate major past earthquakes with specific structures (Pantosti and Valensise 1990; Cello et al. 2003; Galli et al. 2006; Spina et al. 2008; Brozzetti et al. 2009; Villani and Pierdominici 2010; Brozzetti et al. 2017a). These same studies highlight that the kinematics of the Quaternary faults and the focal mechanisms of the major earthquakes are mutually consistent and are compatible with an SW-NE direction of extension (RCMT and TDMT databases by Pondrelli, 2002 and Scogliamiglio et al. 2006).

The area investigated in this work and the structures bounding the Campotenese basin have been pointed out recently in more detail by Brozzetti et al. (2017a), in the frame of a larger study of the Quaternary and active fault pattern on the Calabria-Lucania border (Fig. 1b,c). In the region, three main sets of normal faults have been mapped: a western one, consisting of east- to NNE-dipping faults (red lines in Fig. 1b), and two other main sets of W-to SW-dipping fault segments (blue lines in Fig.1b). The Campotenese Fault (VCT) is the westernmost splay of a SW-dipping fault referred to as Rotonda - Campotenese fault, which develops in a N160E average strike-direction and includes several right-stepping en-echelon segments (Fig. 1b). The VCT extends from the southern border of the Mercure basin to the SW boundary of the Campotenese basin (average strike ~N155E) for ~15 km. Across its northern segment, an associated throw of ~120 m has been assessed based on the displaced stratigraphic boundaries mapped within the bedrock (passage between Triassic dolostones and Jurassic limestones). In this same sector, prevailing dip-slip kinematics has been documented by Brozzetti et al. (2017a). Along the east side of the Campotenese basin, the VCT is generally buried by Holocene deposits, but its localization can be inferred based on stratigraphic observations and geomorphic features, such as sharp ridge fronts, linear scarps, and slope breaks. The VCT controls the distribution and thickness of the clastic fill basin (Middle Pleistocene-Holocene in age, according to Schiattarella et al. 1994) that reaches the maximum thickness (> 30 m) in the western sector (VCT hanging wall, see boreholes stratigraphy at http://sgi2.isprambiente.it/mapviewer/) whereas is very thin (generally < 2-3 m) in the eastern one. The spatial relationships, at surface and depth, between the Quaternary fault segments, and the hypocenters of the re-located events of the 2010-2014 seismic activity (Totaro et al. 2015; Brozzetti et al. 2017a; Napolitano et al. 2020, 2021; Pastori et al. 2021) suggest that the VCT is a good candidate as a seismogenic source for the Mw 5.2 (2012, October 25) Mormanno mainshock. In addition, the analysis of the historical seismicity highlights that the epicenter of the Mw 5.5, 1708 earthquake (Rovida et al. 2020) is located within the VCT hanging wall block, close to its northern termination, leading to hypothesize the possibility of a common seismogenic source with the Mormanno 2012 event.

https://doi.org/10.5194/se-2021-75
Preprint. Discussion started: 14 June 2021


Solid Earth Discussions

Ultimately, based on the available data (e.g. Brozzetti et al. 2017a), the VCT must be considered an active and seismogenic fault, whose size (length of surface trace and depth of detachment) provides an estimate of seismogenic potential much greater than that released over the last few centuries, thus capable of giving surface faulting in the future. Following this line of reasoning, it is hypothesized that some strong paleo-earthquakes, unknown to date, may have caused, along the VCT trace, coseismic surface breaks that are currently no longer visible as they have been leveled by erosion and anthropogenic activity. The search for evidence of such possible paleo-ruptures is therefore a fundamental first step to define the actual seismogenic potential of the VCT and perhaps, to try filling in the Pollino seismic gap.

FIGURE 1 HERE

3. Methodology

Ground Penetrating Radar (GPR) is a high-resolution geophysical method able to provide detailed images of the shallow sub-surface. This methodology is based on the recording of Em echoes, with operative frequencies for geoscience applications generally between 10 MHz and 1000 MHz, depending on the transmitting and receiving antennae. The GPR reflections rise from dielectric permittivity contrasts between the subsurface targets and the surrounding media, which in geological and archaeological applications typically correspond to geo-lithological changes or water content variations (Jol 2009). In "low-loss" materials (Davis and Annan 1989), the investigation depth range is generally within the first ten meters or less. The latter is however controlled also by the electrical conductivity, which for high values causes radar signal attenuation (Annan 2001). The reflections are recorded as a function of the Two-Way-Travel time (TWT) propagation, and displayed as a 1D GPR trace. Several GPR traces displayed along a transect build-up a radar profile or "radargram", that is the 2D representation of the GPR reflections, more commonly identified as the conventional GPR output. A GPR dataset may be provided also as a 3D volume, which has been common for 25+ years in research applications and recently more widespread due to a wider diffusion of commercial GPR instruments equipped with arrays of antennae. The GPR is used in many research and applied fields, such as geological, sedimentological, hydrogeological applications (Bristow and Jol. 2003; Jol 2009), and also in archaeological and engineering studies (Conyers 2006, 2016; Daniels 2004; Goodman and Piro 2013; Utsi 2017). Several 2D/3D GPR studies have already imaged buried tectonic structures. These studies have shown geophysical images of faulting, supporting and/or extending outcrop, borehole, trench data, and contributing to base-knowledge of seismogenic structures as well as to the seismic hazard assessment of several regions around the world. Among the pioneers, we can mention Benson (1995), Smith and Jol (1995), Busby and Merritt (1999), Cai et al. (1996) and Liner and Liner (1997), and on the successive twenty years, other 2D GPR studies were achieved across several faults (Audru et al. 2001; Demanet et al. 2001; Overgaard and Jakobsen, 2001; Bano et al. 2002; Liberty et al. 2003; Reiss et al. 2003; Slater and Niemi, 2003; Malik et al. 2007; Wallace et al. 2010; Yalciner et al. 2013; Imposa et al. 2015; Anchuela et al. 2016; Nobes et al. 2016; Matos et al. 2017; Pousse-Beltran et al. 2018; Zajc et al. 2018; Zhang et al. 2019 and Shaikh et al. 2020). ~~A few GPR surveys have been acquired across Italian normal faults~~ (Salvi et al. 2003; Jewell and Bristow, 2006; Pauselli et al. 2010; Roberts et al. 2010; Ercoli et al. 2013a; Bubeck et al. 2015; Cinti et al. 2015). Over time, ~~such~~ 2D GPR ~~studies~~ were flanked by an increasing number of pseudo-3D or full-3D GPR studies (Grasmueck et al. 2005). Grasmueck and Green (1996) traced the future path of three-dimensional GPR applications, providing a dense 3D GPR volume to image fractures in a Swiss quarry. The study opened the possibility to three-dimensional GPR imaging of subsurface geological structures. Successive studies extended the approach to

https://doi.org/10.5194/se-2021-75
Preprint. Discussion started: 14 June 2021


Solid Earth
Discussions
Open Access
EGU

characterize active faults in different tectonic regimes combining 2D and pseudo-3D GPR surveys (Gross et al. 2000, 2002, 2003, 2004; Green et al. 2003; Horstmeyer et al. 2005; Tronicke et al. 2006; McClymont et al. 2008, 2009, 2010; Vanneste et al. 2008; Christie et al. 2009; Carpentier et al. 2012a,b; Malik et al. 2012; Brandes et al. 2018). A review of the near-surface GPR faulting studies suggests some reflection characteristics as possible indicators for the detection of subsurface fractures and faults (e.g. Smith and Jol 1995; Liner and Liner 1997; Reiss et al. 2003; Gross et al. 2004; McClymont et al. 2008, 2010 and Bubeck et al. 2015). Among these, sharp lateral reflectivity variations, interruptions of the reflections, and the presence of hyperbolic diffractions are considered convincing evidence, as shown also by numerical simulations (Ercoli et al. 2013a; Bricheva et al. 2021). In addition, we have accounted for additional GPR indicators identified for Quaternary faulting in similar environments (Ercoli et al. 2013a,b; 2014; 2015), which are linked to the geometry of stratigraphic deposits across fault zones: i) reflections abrupt truncating and offsetting along sub-vertical discontinuities (especially in the case of a normal fault); ii) reflection packages thickening as they approach the fault strands; iii) abrupt lateral dip variation of the reflections; iv) peculiar reflection package geometries, with contorted reflection patterns resembling *"colluvial wedges"*, which McCalpin (2009) defines as deposit due to "*subsidence and sedimentation of the hangingwall and erosion of the morphological scarp in the footwall*"; v) localized strong GPR signal attenuation due to the presence of conductive media within the main fault zone (possibly associated with colluvial wedges).

Based on the research and criteria reviewed above, we carried out our interpretation of near-surface faulting based on the co-existence of most of these features along several adjacents analyzed GPR profiles. These conditions strengthen the interpretation of each profile and aids to highlight the spatial continuity of the interpreted structures over linear distances of at least many tens, or hundreds, of meters.

3.1 GPR and GNSS survey

The GPR profiles were acquired across the VCT fault (Fig. 1c), during three different geophysical campaigns in the years 2014-2015 (Fig. 2). The entire dataset encompasses 49 radar profiles (linear length of about 4100 m) collected with a Common Offset (CO) configuration.

FIGURE 2 HERE

We used a Zond 12e GPR system equipped with 300 and 500 MHz antennae. The lower frequency antennae was ultimately preferred and considered the best trade-off between maximum resolution and achievable signal penetration (in our case ~ 4 m) concerning the surveyed materials and wanted subsurface structures. The GPR was equipped with an odometer wheel to measure the radar profiles' length and with a Topcon GR-5 Global Navigation Satellite System (GNSS) receiver to achieve accurate positioning of GPR traces and profile. Considering the scarce presence of obstacles across the survey site and the good satellite coverage, we opted for a Network Real-Time Kinematic positioning (NRTK, connected to the NETGEO network), measuring coordinates and elevations with centimetre accuracy, and stored directly within the SEG-Y GPR files.

Three datasets were acquired after preliminary fieldwork and collection of geological structural data at the surface and which allowed us to infer the possible location of the fault trace. The average NE-SW direction of the GPR lines was initially planned with the primary purpose of intersecting the VCT fault ~perpendicularly to its SW-NE strike, as reported by literature and visible by surface evidence. This solution theoretically allows a more reliable interpretation

https://doi.org/10.5194/se-2021-75
Preprint. Discussion started: 14 June 2021


Solid Earth
Discussions
Open Access
EGU

of the investigated structure by reducing the effect of the apparent dip-direction and dip-angle of both stratifications and faults.

The first acquisition carried out in 2014, resulted in twelve SW-NE GPR profiles collected in the southern sector (CMT light-blue lines in Fig. 2a), which was a flat land characterized by Quaternary alluvium. The second acquisition encompassed four additional radar profiles collected in the same area, and another nine radar profiles progressively moving to north, which were collected with slightly different and converging orientations in the central sector (CMT green lines Fig. 2a). This solution was pursued for two main reasons: 1) to avoid directly surveying the outcropping dolostones (only partially crossed with two northernmost profiles) characterizing two hills *h1* and *h2* (dashed white polygons in Fig. 2), thus focussing only on the sedimentary cover which is our target for possible Quaternary faulting; 2) to optimize, using subsurface data, the future acquisition schemes by figuring out the effective "apparent dip" of the geologic structures, to consider in the interpretation of 2D GPR images (similar to the interpretation of reflection seismic profiles).

In order to intercept several possible buried faults and fault-related structures as well as to fully image the local structural setting, the successive 2015 acquisition crossed part of the Triassic dolostones ridge with longer GPR profiles. ~~Preliminary results shown by~~ GPR profiles collected during the second 2014 campaign (close to *h1* and *h2)* revealed a considerable difference in GPR reflectivity between the unconsolidated deposits and layered and fractured Mesozoic lithotypes (Gafarov et al. 2018). Therefore, two new datasets of 24 GPR parallel radar profiles (CMT dark-blue sets of lines in Fig. 2a, *north "n"* and *south "s"*) were extended in NNE-SSW and NE-SW directions, respectively, crossing *h1* for several tens of meters (max profile length ~220 m) throughout the basin. The GPR profiles were recorded using a trace distance of 0.05 m and a profile inter-distance of 10 m for dataset *"n"* and 25 m for dataset *"s"*, respectively. A detailed summary of the acquisition parameters used ~~in the field during~~ the GPR surveys is reported in Table I. For these two new grids, the profile spacing and positioning are more regular and accurate, thanks to a preparatory transects planning using a Geographic Information System Information System (GIS) project. Thus, we later staked out their initial and final positions during the fieldwork through the differential Global Navigation Satellite System (GNSS). The results of the accurate GPR traces positioning achieved during the GNSS campaigns were later used also for GPR data processing, visualization, and interpretation.

TABLE 1 HERE

3.2 GPR data processing and results:

The processing sequence was customized after testing several flows and parameters. We aimed to remove random and coherent (e.g. ringing) noise and enhance the data quality to better visualize the geometry of the buried reflections and their discontinuity in signal amplitude and phase. The first step was an accurate Quality Control (QC) of the profile coordinates and topographic profiles. Although the favorable environmental conditions of the site for a GNSS survey, some measurements were occasionally suffered a degradation of positional accuracy (e.g. temporary scarce satellite coverage or poor communication via Network Transport of RTCM via Internet Protocol - Ntrip). For some traces therefore the coordinates and elevation field records that were outliers were corrected using various strategies (e.g. replacement, interpolation, or smoothing, Figs. 3a,b).

FIGURE 3 HERE

https://doi.org/10.5194/se-2021-75
Preprint. Discussion started: 14 June 2021


Solid Earth
Discussions
Open Access
EGU

We have also compared our measurements with topographic transects extracted from a 10 m and a 5 m resolution Digital Terrain Models (DTM) by Tarquini et al. (2012) and by Regione Calabria. Later on, we finally used a 1 m resolution DTM (Geoportale Nazionale, Lidar data provided by Italian Ministero dell'Ambiente e della Tutela del Territorio e del Mare - MATTM) to double-check if, despite the different scales of observation, the topographic profiles were comparable. Although the metre resolution of the DTM is unable to represent centimetre topographic variations, the comparison confirmed an excellent match of the topographic profiles at a meter scale, so that the DTM data were integrated to correct the GNSS measured topography when the accuracy of GNSS recordings were excessively degraded. With the topographic profiles corrected, the raw GPR data (Fig. 3c, illustrating the profile cmt5s) were initially processed with the Prism software (Radar System, Inc., http://www.radsys.lv/en/index/) using a basic processing sequence, to analyze the main characteristics of data and optimize a customized processing flow. The processing sequence was later improved through ReflexW software (https://www.sandmeier-geo.de/reflexw.html, see Table II for details on the processing algorithms and parameters). The workflow included a time-zero correction, dewow, amplitude recovery, velocity analysis, background removal, bandpass filtering, F-K filtering, 2D time migration, topographic correction, and time-to-depth conversion. The amplitude recovery was operated through a "gain function" including by a linear and an exponential coefficient ($g(t)=(1+a*t)*e^{(b*t)}$) to enhance the amplitude (reflectivity) contrasts as well as preserving the horizontal and vertical amplitude variations already visible in the raw data (Fig. 3a). This amplitude recovery function was used across all the profiles with slight customization depending on the datasets (details in table II). The entire processing flow was applied to all the available radar profiles, again with occasional filtering adaptations aiming to remove local pervasive signal ringing (e.g. due to low antennae-ground coupling). Particular care was dedicated to the migration process, whose algorithm was decided after extensive tests on several radar profiles to select the best migration strategy.

TABLE 2 HERE

In fact, a very different reflectivity and maximum depth of penetration are visible in the data: it is more than 150 ns in the central sector, reducing to 70-80 ns in the rest of the radar profiles (Fig. 3c): this fact suggests sharp lateral variations of subsurface media (Figs. 3d) and possibly of the velocity field. Thus, we have first tested a 1D time migration algorithm (Kirchhoff) performing a Migration Velocity Scan (MVS) analysis (Forte and Pipan 2017) and inspecting the success of diffraction hyperbola collapse after migration. We have varied constant values of Em velocity, from a minimum of 0.06 up to 0.12 m/ns, with steps of 0.01 m/ns, to evaluate considerable variation in dielectric properties of surveyed media. The MVS highlighted a higher velocity for the central sector of the GPR profiles which displays high reflectivity: Fig. 4 illustrates an extract of the migration results obtained on the profile cmt1n_a, by using three constant values of average velocity. The profile in Fig. 4a shows the unmigrated version characterized by numerous hyperbolic and half hyperbolic diffractions originated by single scatter points and wavy reflections (white arrows). In Fig. 4b we display the first test using v = 0.07 m/ns, showing overall good results, with slightly under-migration at a few points mainly located within the shallower sediments (light-blue arrows). The hyperbolic diffractions are also nicely collapsed using higher velocity (v = 0.09 m/ns) as shown in Fig. 4c (dark-blue arrows), even if some imaging problems are rising on deeper reflections. The last migration scan test (v =0.11 m/ns) displays a good result only in few profile sectors (dark-blue arrows), particularly localized within the sectors with high reflectivity, displaying an improved lateral reflection continuity. The rest of the radar profile shows general poor

https://doi.org/10.5194/se-2021-75
Preprint. Discussion started: 14 June 2021

imaging, particularly in the area characterized by strong attenuation, where the wavy reflection is clearly over-migrated (red arrows indicating migration smiles, Fig. 4d).

FIGURE 4 HERE

The workflow, therefore, suggests a challenging imaging task, due to velocity variation happening not only in depth as well as laterally across the different media. This sharp change of reflectivity and velocity at a distance of about 13-14 m (Fig. 4d) represents a complex problem for the efficiency of 1D migration algorithms standardly used for GPR imaging. Such considerations have driven to test a 2D migration algorithm, by creating and using a 2D velocity model obtained for each radar profile through a hyperbolic diffraction fitting tool (Fig. 5a). Single velocity points have been fitted for each area clearly displaying hyperbolic diffractions, while in the remaining parts of the radar profiles we have arbitrarily included presumed velocity adaptation only to obtain a regular grid of points to spatially interpolate the 2D models. The 2D migrated radar profiles, in comparison to the 1D approach, resulted in improved imaging of GPR profiles, displaying a more accurate collapse of the hyperbolic diffractions into point sources and an improved relocation of dipping reflections, with a refinement of their geometry and an increase of their continuity. A good-quality imaging result is visible on the central sectors of radar profiles displaying strong reflectivity and reflections with improved continuity, but also many phase breaks and displacements. Despite steep topographic gradients, sharp lateral velocity variation and the reflection heterogeneity might cause imaging issues to be treated using more specific workflows (Lehmann and Green, 2000; Heincke et al. 2006; Goodman et al. 2007; Dujardin and Bano 2013), we believe we have reached a good compromise for our purposes. In our case, a considerable improvement, can be seen along the hill-slope and flatter areas (profile cmt1n_a, Fig. 5b) which are of greatest interest for the study aimed at detecting possible earthquake ruptures within the Quaternary deposits. The improved imaging of reflection geometries is therefore fundamental for the interpretation and detection of geophysical signatures of faults.

FIGURE 5 HERE

A successive import of the processed SEG-Y was done into the seismic interpretation software OpendTect Pro v.6.4 (Academic license courtesy of dGB Earth Science, https://www.dgbes.com), which was used first for global quality control of processing operations (correctness of topographic correction and datum plane, coordinates accuracy and matching, profiles orientation and intersection) and for three-dimensional (3D) visualization of all the profiles (Fig. 6a).

The three-dimensional GPR project was subsequently integrated with geological and structural maps, DTM, and literature schemes (using a common Coordinate Reference System: WGS84 UTM Zone 33N, EPSG: 32633) in the Move suite software v. 2019.1 (Academic license courtesy of Petroleum Experts, https://www.petex.com/) for the GPR interpretation and model building. All the east and west-dipping fault surfaces were created interpolating the fault-sticks picked on displaced reflections and correlated across adjacent radar profiles. In particular, we used the "*surface geometry*" tool to extract the properties of each single mesh building up the surfaces, and obtaining the "dip" and "dip azimuth" data. Subsequently, such values have been automatically saved in an attribute table, which can then be queried to reconstruct the “synthetic” stereonets.

4. GPR data description and interpretation

https://doi.org/10.5194/se-2021-75
Preprint. Discussion started: 14 June 2021

The 3D MOVE project allowed us to extract 2D and 3D visualizations of the radar profiles acquired across the VCT fault trace and allows us to better figure out the relationships between the main reflections identified on the different GPR data (Fig. 6a). The workflow aimed to reconstruct and model the three-dimensional surfaces including horizons and high-angle discontinuities.

FIGURE 6 HERE

A common feature on all the radar profiles is the strong reflectivity visible within their central sectors (profile cmt3n, Fig. 6b), which are characterized by a more irregular and steeper slope, particularly within the northern portion of the surveyed area. These sectors with deep penetration areas are caused by the Triassic dolostones, which outcrop in the central and northern portions of the study area (Figs. 1c and 2a). In the southern side of *h1*, thin microbialitic laminae allows one to measure the attitude of the bedding, which shows a NNW dip (~ 30-35°). In the same area, we measured two sets of major and minor joints, both with a dip angle of ~ 40-45 ~~degrees~~ and a SW and SE dip, respectively. Looking at the quality of the radar reflections and at the remarkable depth (~ 6 m, Fig. 6b) reached by the GPR signal, this rock type represents an excellent dielectric medium (corresponding to higher frequency content zone in the 2D spectrum of Fig. 6c). However, its reflection pattern is not spatially homogenous, being often characterized by oblique and sub-parallel reflections interpretable as dolostone beds, displaying moderate (25-30°) west and east "apparent" dip on the respective sides of the surveyed dolostone hills. In addition, these reflections are frequently cut and slightly displaced by apparent high-angle (60-65°) phase discontinuities, also highlighted by a dense hyperbolic diffractions pattern (radar profile cmt2n, Fig. 7a), interpreted as sets of joints or minor faults fracturing and displacing the dolostone layers (Fig. 7b). Apart from its internal heterogeneities, the GPR signature of the Triassic dolostones can be considered as a well-defined depositional facies (*fc1*) (Sangree and Widmier 1979; Huggenberger 1993; Beres et al. 1999; Jol and Bristow 2003). This radar signature was recorded not only in correspondence of the outcropping carbonates but also in the transition slope areas, where just a thin soil layer or a scarce sedimentary cover was present onsite (Figs. 7b,c). A different GPR facies (*fc2*) is characterized by laterally-continuous and sub-parallel prominent reflections in the very shallow depth, just beneath the direct arrivals (< 1 m), which stratigraphically seals the underlying reflections; more discontinuous, wavy and contorted reflections of moderate to low reflectivity are visible in the 1-3 m depth-range (variable across the analyzed profiles) onlapping onto a generally prominent and wavy reflection (Figs. 7a,b). Below this reflection pattern (~ 2-3 m), the signal strongly attenuates. Summarizing~~-~~, the shallower reflections packages show continuous beds dipping parallel to the slope, but under these, the slightly deeper reflections are less continuous, displaying variable dip and locally a contorted pattern, with numerous diffraction hyperbolas (in unmigrated data, Fig. 7a) as well as important lateral amplitude variations (Fig. 7b).

FIGURE 7 HERE

We have classified the overall radar signature of these reflection packages as facies *fc2*, corresponding to the alluvial/colluvial deposits (Fig. 7b,c,d) outcropping on the flatten sectors, which represent the GPR profile sectors we've carefully inspected to find for geophysical evidence of Quaternary faulting. A key-layer for this research is in our opinion the described wavy reflection, recognized in several radar profiles. This prominent reflection shows frequently a stepped geometry, with frequent breaks of its continuity and lateral depth variations; moderate to strong signal attenuation generally underlies this reflection. The related interpretation is not straightforward in the absence of direct data (e.g. boreholes and/or paleoseismological trenches) or at least without additional geophysical data. A

https://doi.org/10.5194/se-2021-75
Preprint. Discussion started: 14 June 2021


Solid Earth
Discussions
Open Access
EGU

strong reflection suggests significant variation of a dielectric constant between the two media so that most of the incident energy is reflected back to the receiver at the surface, which is potentially explained by several geological models, such as: i) a high dielectric contrast may be a result of a sharp soil moisture variation (Ercoli et al. 2018); ii) a sharp erosional, stratigraphic or tectonic boundary within heterogeneous deposits (Ercoli et al. 2015), or iii) a contact between two considerably different lithologies, such as unconsolidated deposits laying above a bedrock substrate (e.g., Frigeri and Ercoli 2020) reflecting back all (or almost all) the incident signal. In addition, the possible role of conductive sediments within layered deposits (e.g. high clay content) should not be discounted, and it might explain localized strong signal attenuation.

~~To support~~ the GPR data interpretation~~, some suggestions for consideration are~~: 1) stratigraphy of two water-wells located only ~2.5 km away on the north-westernmost sector of the Campotenese basin (Brozzetti et al. 2017a); 2) geomorphological and geological data achieved through aerial-photo interpretation and field study on the surrounding landscape (Brozzetti et al. 2017a); 3) the geometrical characteristics shown by this reflection and of the underlying reflection pattern visible in the processed data.

The available well logs show the Pleistocene-Holocene alluvium and colluvium layered above the carbonate bedrock ~20-30 m depth (Brozzetti et al. 2017a), a greater depth than the strong GPR reflection. However, it should be observed that the drilled area is located over the depocenter of the basin whereas the studied GPR site is placed just on its eastern border, in proximity to emerged calcareous hills. In addition, it should be mentioned that only terraced Middle-Pleistocene silts and sands (Schiattarella et al. 1994) and slight coatings of Late Pleistocene colluvium (generally < 2 m thick) are documented to outcrop in the eastern sector of the basin (footwall of VCT fault) (see Fig. 7 in Brozzetti et al. 2017a).

The subsurface geometries highlighted by the GPR profiles suggest a relatively thin layer of sedimentary deposits resting on a fractured substratum, whose top surface is progressively deepening towards the west, thus providing increased space for settling sediments. For this reason, a gradual deposits thickening is observed from east to west. Therefore, we interpret the prominent and wavy GPR reflection as a buried top layer of carbonate (e.g. as observed by Bubeck et al. 2015), in our case the Upper Triassic dolostones formation lying beneath shallow and poorly consolidated Quaternary deposits. Thus, in this surveyed sector of the basin, we interpret the dolostone top to be located not ~20-30 m deep as in the noth-westernmost area, but at a shallower depth (1-3 m) below the topographic surface and across both two sides of the surveyed hills. After picking this strong reflection in all the radar profiles, we have therefore reconstructed the top of bedrock surface (Fig. 8a).

We can now focus on the structural interpretation by analyzing the geophysical characteristics of this strong reflection. As illustrated by a recent structural map of the basin in Fig. 8a (modified after Brozzetti et al. 2017a), the area is dissected by a set of en-echelon fault splays connected to the VTC master fault. The strong reflection interpreted as the dolostone top shows a clear "stepped" geometry (Figs. 5b-6b-7b-8b), highlighting abrupt lateral variations in depth and in its thickness (sediment growth and onlaps). We also notice other geophysical features, which can be observed in the stratigraphy of overlying deposits fc1: some reflections are semi-continuous to discontinous (sharp variation in signal amplitude and phase), displaying lateral dip variation.

FIGURE 8 HERE

In some sectors these broken reflection packages present truncantions (Smith and Jol 1995), vertical offset, and hyperbolic diffraction events. Contorted reflections across the main discontinuities frequently show localized strong

https://doi.org/10.5194/se-2021-75
Preprint. Discussion started: 14 June 2021

attenuation of GPR signal (interpretation summarized in caption of Fig. 8b), which might be linked to their high dip-angle, causing a minor amount of energy being reflected back to the antenna, but more likely, due to the presence of conductive fine soils across faulted zones (e.g. circles 1 and 2 in Fig. 8b). These conditions can be linked to different depositional facies across fault zones (McClymont et al. 2010) e.g. including colluvial wedges (Reiss et al. 2013; Bubeck et al. 2015). Such peculiar GPR signature is therefore compatible with possible co-seismic displacement due to Late Quaternary surface faulting events (Fig. 8b). Using such stratigraphic evidence and geophysical markers of faulting, we have therefore interpreted and classified synthetic (west-dipping, blue) and antithetic (east-dipping, red) normal faulting events within the Quaternary sediments (Fig. 8b). The interpreted faults present a dip angle between 65-75° and a vertical offset ranging from a few tens of centimeters up to ~1 meter, and were picked using solid lines (fault sticks). During the interpretation process, when the presence of geophysical markers of faulting were uncertain, a dashed fault segment has been initially added and only later analyzed a second time by looking at their possible connection with nearby lines. In addition to the fault sticks within the Quaternary sectors, we placed main fault sticks across the sharp boundary between the Triassic dolostone and the Quaternary sediments. The contact is generally characterized by fractured zones including hyperbolic diffractions (in unmigrated data), contorted reflections geometry of variable dip angle, abrupt truncations marked by sharp lateral variation of the reflectivity due to localized attenuation (Figs. 3 to 9).

By interpolation of the fault sticks placed in adjacent profiles, we have created the fault surfaces that show a good degree of continuity, from north to south (Fig. 9).

Our geophysical interpretation allowed reconstructing the fault-network and the geometry of the associated synsedimentary deposits, at a higher resolution (Fig. 9). The 3D map views of Fig. 9 show a structural scheme of the main fault lineaments displaying a NW-SE strike. Our interpretation highlights an en-echelon system of main SW and NE-dipping faults on both sides of the hills where the Triassic dolostones crop out, as well as several secondary structures within the Quaternary sediments.

5. Discussion

5.1 Inferences from subsurface 3D model

The high-angle GPR discontinuities identified in the study, dissecting not only Quaternary alluvial-colluvial deposits but also ~~deeper reflections referred to~~ deeper stratigraphic layers, show a considerable continuity in the NW-SE direction (Fig. 9). These structures can be interpreted as the surface expression of an articulated set of extensional meso-faults associated with the VCT.

The reconstructed faults are arranged in a horst-graben structure in which the higher displacements are associated to the west-dipping faults (Fig. 9). Among these faults, the master structure in the southern sector of the basin (Fig. 9a) bound toward west a structural high where the Triassic dolostones crop out. The structural high, which corresponds to a topographic high elongated in the NNW-SSE direction, is also bordered towards the east by a minor east-dipping normal fault (Fig. 9b). Thus, it appears as an uplifted horst showing an axis of elongation sub-parallel to the average strike of the Campotenese basin. The horst is mostly buried within the basin but locally emerges from the Quaternary sediments, as in the central portion of the investigated area (*h1* and *h2* in Fig. 2a).

The fault-set d1 in Fig. 9c shows the maximum displacements and the most evident deformations of the adjacent sub-surface deposits. It can be considered a splay of the VCT (Fig. 8b), separated by a right step-over of about 0.5 km from the main segment that borders the eastern basin (Figs. 2c, 8a).

https://doi.org/10.5194/se-2021-75
Preprint. Discussion started: 14 June 2021


Solid Earth
Discussions
Open Access
EGU

The three-dimensional model (Fig. 9a,c) highlights that these faults, despite having an average NW-SE direction, are characterized by a complex polymodal pattern of strikes, with NS sections alternating to NW-SE sections. The character, which is observed at various scales, both along the entire VCT and along all the extensional structures of the area (Brozzetti et al. 2017a), is also confirmed by the statistical analysis of the reconstructed fault planes reported in the stereo plots of Fig. 9d (d1-d3= west-dipping faults; d2-d4= east-dipping faults).

FIGURE 9 HERE

The variations of thickness of the Quaternary deposits, detectable on the radar profiles, are consistent with the horst and graben configuration. Thinning is observed in correspondence with the raised buried blocks whereas thickening and wedge-shaped and locally chaotic geometries occur in correspondence with the lowered blocks. These latter features are only associated with west-dipping faults, thus enhancing the role of this fault set (Fig. 8b), and the syn-tectonic nature of the Late Quaternary sedimentation.

5.2 Seismic hazard implications

In many cases, seismological data show that the outcropping Quaternary faults are capable of releasing earthquakes, but the maximum expected magnitude is not well constrained. An estimate of can be made using well-known scale-relationships (Wells and Coppersmith 1994; Wesnousky et al. 2008, Leonard 2010, Stirling et al. 2013) with knowledge of the geometric parameters (e.g. fault length, area and depth), which are often difficult to assess. These scale relations can be applied also on scarps originated by cumulated coseismic surface faulting events of medium-strong earthquakes (generally M > 6), possibly distinguishing the amount of slip due to each event through paleoseismological analysis. But in the case of VCT, no direct information is available on the nature of the surveyed deposits, and their accurate dating has not been carried out at the present day. The interpretation of our GPR data confirms the segmentation of the VCT and point out the presence of a buried splay, which appears to have exerted a strong control on the deposition of Late Quaternary sediments, just below the present topographic surface. Moreover, we have highlighted that the sediments, in turn, are affected by faulting. Their location at a very low depth (1 - 4 m) in a flat land of an intra-mountain basin which is presently undergoing alluvial and colluvial sedimentation, suggests their attribution to the Holocene. Thus, pointing out normal faulting of Holocene deposits would be, in itself, a very important result for the Campotenese area, ~~as no previous study has provided this kind of evidence yet. In fact,~~ a Middle-Late Pleistocene age of activity was suggested for the Mercure and Campotenese boundary faults by Schiattarella et al. (1994) and Brozzetti et al. (2017a), based on morpho-structural observations, ~~whereas~~ their Holocene activity had been only inferred ~~according to the~~ possible associations of the faults with the recent 2010-2014 Pollino seismic sequence (Brozzetti et al. 2017a).
Our data seem even more promising because the GPR facies interpretation highlights the possible presence of small-scale grabens or half-graben and fault-related coseismic-wedges (e.g. as observed by Reiss et al. 2013 and Bubeck et al. 2015), at shallow depth (just below the present agricultural soil). This inference would testify to not only the persistence of extensional deformations up to the very Late Quaternary but would even imply the occurrence of episodes of surface faulting, proving new perspectives on the actual seismic hazard of the area. In other words, the Campotenese basin may have been affected in the relatively recent past by medium-strong earthquakes, nucleated from the VCT, capable of producing ~~surface~~ coseismic scarps, ~~which~~ were subsequently erased by footwall erosion and sedimentation at the hanging wall.

https://doi.org/10.5194/se-2021-75
Preprint. Discussion started: 14 June 2021

The hypothesis of past earthquakes, with a magnitude sufficiently high to cause surface ruptures in this area, sounds reasonable if we consider that historical events with $6 < M_w < 7$ are documented a ~~little~~ further (~50 km) north and south (Fig. 1a) (~~Guidoboni et al. 2018~~),

Some paleoseismological earthquakes with inferred magnitude ~~up to~~ M_w = ~~7~~ are attributed to the Castrovillari fault, located at about 20 km to SE and also falling within the Pollino seismic gap (Cinti et al. 1997; Michetti et al. 1997; Cinti et al. 2002, 2015; ~~and Ercoli et al. 2015~~).

The estimates of the VCT fault-length (~~Brozzetti et al. 2017a~~) provide an overall value of 15 km which is compatible with the maximum expected magnitudes capable to produce surface breaks. From using earthquake scaling relationships based on coseismic rupture-length, as the main computation parameter, the obtained magnitudes are in the range of 6.45 (Wells and Coppersmith 1994) to 6.8 (Wesnousky et al. 2008; Leonard 2010) in the case of a complete rupture of the VCT fault. The result suggests that the most recent earthquakes that have affected the study area (2012 - M_w 5.2; 1894 - M_w 5.1; 1708 - M_w 5.8 and perhaps 1693 - M_w 5.6) have a source at ~ 8 km depth (Totaro et al. 2015; Brozzetti et al. 2017a; Napolitano et al. 2020 and 2021, Sketsiou et al., 2021). Thus, the seismic energy released is likely too low for an active fault set as well as not enough to be causative of the buried VCT ruptures detected. Because historical catalogs do not show events with $M_w > 6$ (~~Guidoboni et al. 2018~~), probably a very energetic earthquake could have occurred before the period covered by the available seismological catalogs. In this context, the area needs more investigations to verify if an event with M>6 can repeat in the ~~near~~ future, as suggested by the recurrence times of strong earthquakes generated by the typical Apennine extensional faults, specifically ~ 4 ky for this region (Galli 2020). Our study, points out the need of extending our detailed reconstruction of the buried segments of the VCT, both along- and across-strike, and not only in the surveyed sector, but also on segments bounding the northern edge up to the Mercure basin. In addition, our results may also be useful and preparatory for orienting and locating further campains, integrating other geophysical tools, and possibly paleoseismological trenches, drilling and sampling for dating (e.g., luminescence, radiocarbons, etc).

Such investigations could help to address the following crucial points, namely: i) ground truthing the presence of such past coseismic surface breaks along the VCT, ii) define their timing, iii) obtain a recurrence time for the most energetic events, and ultimately iv) aid a quantitative evaluation of the probability that a strong earthquake could hit the area in the near future.

6. Conclusions

Our workflow allowed for the creation of a detailed 3D model which reconstructs the near-surface pattern of paleoseismic ruptures across an area straddling the VCT active fault across the Campotenese continental basin (Mt. Pollino region). Based on previous geological mapping, the VCT in southern section of the study area was hypothesized to be buried under a clastic Holocene cover.

We have used non-destructive GPR survey, a powerful tool to investigate the shallow geological structures. The processing, analysis, assemblage, and interpretation of the 49 GPR profiles was pursued using expertise, techniques, and tools borrowed from reflection seismic industry applications. The use of GPR has allowed us to quickly investigate the study area with low costs, in a non-destructive manner and without special authorizations. A relatively fast pseudo-3D GPR survey operated during four days of team fieldwork was an efficient compromise between spatial coverage of the study site and duration of the acquisition. On the other hands, the data processing was non-trivial, requiring about six months overall to set up an optimized workflow, due to challenging characteristics like the steep and rugged

https://doi.org/10.5194/se-2021-75
Preprint. Discussion started: 14 June 2021

topography as well as sharp lateral variations of geophysical properties of media (Triassic Dolostones vs Quaternary deposits).

More in detail of the study area, our structural reconstruction shows several sets of sub-vertical discontinuities (1-4 m depth range), which we interpreted as extensional ~~surface~~ faulting, bounding small local "graben or semi-graben-like" structures located within Holocene sediments and down to underlying dolostones. We have also identified some chaotic and laterally discontinuous GPR-stratigraphic facies, interpreted as near-fault deposits (i.e. colluvial wedges ?). These structures suggest the possibility that surface faulting occurred in relatively recent times, but its traces were successively leveled by the concurrent natural processes of erosion, aggradation and, anthropogenic activities. All these buried features suggests that past strong earthquakes ($6 < M_w < 7$) might have occurred in the study area, which is located within the central sector of the well known "Mt. Pollino seismic gap". As in the time range covered by the historical seismological catalogs there is no record of such energetic events, we hypothesize that the area could be at ~~high risk~~ of occurrence of a strong earthquake. We ~~hope~~ the primary effect of our work is to raise the level of attention regarding the seismic hazard in the Campotenese area, thus prompting further research to achieve an improvement of the base-knowledge for assessing its seismogenic potential. We firmly promote a more widespread use of our GPR workflow, particularly where near-surface data are scarce, as a base study for other seismic gaps worldwide.

Acknowledgments

The study has benefited from funding sources: Agreement INGV-DPC 2012-2013 & 2014-2015, Project S1 – Miglioramento delle conoscenze per la definizione del potenziale sismogenetico - Base-knowledge improvement for assessing the seismogenic potential of Italy, https://sites.google.com/site/ingvdpcprojects1/home, resp. Cristina Pauselli, funded by Italian Presidenza del Consiglio dei Ministri – Dipartimento della Protezione Civile (DPC). The paper does not necessarily represent DPC official opinion and policy. We sincerely thank Leonardo Speziali, Prof. Costanzo Federico, and Roberto Volpe for their support during the field operations, as well as Khayal Gavarof for his valuable collaboration in data processing. We thank QGIS (https://www.qgis.org/it/site/) for providing the software with an open-source license, Petroleum Experts (https://www.petex.com/products/move-suite/), and dGB (https://www.dgbes.com/) for providing the academic licenses MOVE and OpenDtect software. We acknowledge NETGEO for academic access to the NRTK network (http://www.netgeo.it/). We would also like to thank the Ministero dell'Ambiente e della Tutela del Territorio e del Mare (MATTM) and the Regione Calabria for providing free access to geospatial data such as DTM and aerials (Regione Calabria - www.regione.calabria.it, under license IODL 2.0. - https://www.dati.gov.it/iodl/2.0/). The paper is the results of collaboration within the framework of the Interuniversity Center for 3D Seismotectonics with territorial applications - CRUST (https://www.crust.unich.it/). The GPR dataset presented in this study is available on request from the corresponding author.

https://doi.org/10.5194/se-2021-75
Preprint. Discussion started: 14 June 2021

References

Amicucci, L., Barchi, M.R., Montone, P., and Rubilani, N.: The Vallo di Diano and Auletta extensional basins in the southern Apennines (Italy): a simple model for a complex setting, Terra Nova, 20, 475-482, https://doi.org/10.1111/j.1365-3121.2008.00841.x, 2008.

Amodio Morelli, L., Bonardi, G., Colonna, V., Dietrich, D., Giunta, G., Ippolito, F., Liguori, V., Lorenzoni, S., Paglionico, A., Perrone, V., Piccarreta, G., Russo, M., Scandone, P., Zanettin-Lorenzoni, E., and Zuppetta, A.: L'Arco calabro peloritano nell'orogene appenninico-maghrebide, Mem. Soc. Geol. It., 17, 1-60, 1976.

Anchuela, Ó.P., Lafuente, P., Arlegui, L., Liesa, C. L., and Simon, J. L.: Geophysical characterization of buried active faults: the Concud Fault (Iberian Chain, NE Spain), Int J Earth Sci (Geol Rundsch), 105, 2221–2239, https://doi.org/10.1007/s00531-015-1283-y, 2016.

Annan, A.P.: Ground-penetrating radar workshop notes, Sensors and Software Inc. Mississauga, ON, Canada, 192 pp.., 2001.

Ascione, A., Cinque, A., Santangelo, N., and Tozzi, M.: Il Bacino del Vallo di Diano e la tettonica trascorrente plio-quaternaria: nuovi vincoli cronologici e cinematici, Stud. Geol. Camerti, 1992/1, 201– 208, 1992a.

Audru, J.C., Bano, M., Begg, J., Berryman, K., Henrys, S., and Niviere, B.: GPR investigations on active faults in urban areas: the Georisc-NZ project in Wellington, New Zealand, Comptes Rendus de l'Academie des Sciences - Series IIA, Earth planet. Sci., 333(8), 447-454, https://doi.org/10.1016/S1251-8050(01)01663-9, 2001.

Bano, M., Edel, J.-B., Herquel G., and EPGS class 2001/2002: Geophysical investigation of a recent shallow fault, The Leading Edge, 21 (7), 648-650, https://doi.org/10.1190/1.1497317, 2002.

Barchi, M.R., Lavecchia, G., Galadini, F., Messina P., Michetti, A. M., Peruzza, L., Pizzi, A., Tondi., E., and Vittori, E.: Sintesi delle conoscenze sulle faglie attive in Italia Centrale: parametrizzazione ai fini della caratterizzazione della pericolosità sismica, CNR-GNDT, Projects 5.1.2, 6a2, 5.1.1, Esagrafica, Roma, 2000.

Bello S., de Nardis R., Scarpa R., Brozzetti F., Cirillo D., Ferrarini F., di Lieto B., Arrowsmith R. J., Lavecchia G.: Fault Pattern and Seismotectonic Style of the Campania – Lucania 1980 Earthquake (Mw 6.9, Southern Italy): New Multidisciplinary Constraints", Frontiers in Earth Science, 8, 652, https://doi.org/10.3389/feart.2020.608063, 2021.

Benson, A.K.: Applications of ground penetrating radar in assessing some geological hazards: examples of groundwater contamination, faults, cavities, Journal of Applied Geophysics, 33(1–3), 177–193, https://doi.org/10.1016/0926-9851(95)90040-3, 1995.

Beres, M., Huggenberger, P., Green, A. G., and Horstmeyer, H.: Using two- and three-dimensional georadar methods to characterize glaciofluvial architecture, Sediment. Geol., 129, 1-24, 1999.

Boncio, P., Pizzi, A., Brozzetti, F., Pomposo, G., Lavecchia, G., Di Naccio, D., and Ferrarini, F., Coseismic ground deformation of the 6 april 2009 L'Aquila earthquake (central Italy, Mw 6.3), Geoph. Res. Lett., 37, http://dx.doi.org/10.1029/2010GL042807, 2010.

Brandes, C., Igel, J., Loewer, M., Tanner, D., C., Lang, J., Müller, K., and Winsemann, J.: Visualisation and analysis of shear-deformation bands in unconsolidated Pleistocene sand using ground-penetrating radar: Implications for paleoseismological studies, Sedimentary Geology, 367, 135-145, https://doi.org/10.1016/j.sedgeo.2018.02.005, 2018.

Bricheva, S.S., Dubrovin, I.O., Lunina, O.V., Denisenko, I.A., Matasov, V.M., Turova, I.V., Entin, A.L., Panin, A.V., and Deev, E.V.: Numerical simulation of ground-penetrating radar data for studying the geometry of fault zone, Near Surface Geophysics, Accepted Author Manuscript, https://doi.org/10.1002/nsg.12153, 2021.

https://doi.org/10.5194/se-2021-75
Preprint. Discussion started: 14 June 2021

611 Bristow, C.S., and Jol, H.M.: GPR in sediments: advice on data collection, basic processing and interpretation, a good
612 practice guide, In: Ground Penetrating Radar in Sediments, (Eds C.S. Bristow and H.M. Jol) Geol. Soc. Spec. Publ.,
613 211, 1-7, https://doi.org/10.1144/GSL.SP.2001.211.01.02, 2003.
614 Brozzetti, F., and Lavecchia, G.: Seismicity and related extensional stress field: the case of the Norcia Seismic Zone
615 (Central Italy), Ann. Tectonicae, 8(1), 36–57, 1994.
616 Brozzetti, F., Lavecchia, G., Mancini, G., Milana G., and Cardinali, M.: Analysis of the 9 September 1998 Mw 5.6
617 Mercure earthquake sequence (southern Apennines, Italy): a multidisciplinary approach, Tectonophysics, 476, 210-
618 225, https://doi.org/10.1016/j.tecto.2008.12.007, 2009.
619 Brozzetti, F.: The Campania-Lucania extensional fault system (southern Italy): a suggestion for a uniform model of
620 active extension in the Italian Apennines, Tectonics, 30 (5), 1-26, TC5009, http://dx.doi.org/10.1029/2010TC002794,
621 2011.
622 Brozzetti, F., Cirillo, D., de Nardis, R., Lavecchia, G., and Cardinali, M.: Detailed mapping of active faults in the
623 Calabro-Lucania Region, Report INGV-DPC 2014-2015 project S1 "Base-knowledge improvement for assessing the
624 seismogenic potential of Italy, https://sites.google.com/site/ingvdpcprojects1/home, 2015.
625 Brozzetti, F., Cirillo, D., de Nardis, R., Cardinali, M., Lavecchia, G., Orecchio, B., Presti D., and Totaro, C.: Newly
626 identified active faults in the Pollino seismic gap, southern Italy, and their seismotectonic significance, J. Struct. Geol.,
627 94, 13-31, https://doi.org/10.1016/j.jsg.2016.10.005, 2017a.
628 Brozzetti, F., Cirillo, D., Liberi, F., Piluso, E., Faraca, E., De Nardis, R., and Lavecchia, G.: Structural style of
629 Quaternary extension in the Crati Valley (Calabrian Arc): Evidence in support of an east-dipping detachment fault, It.
630 Journ. of Geosci., 136(3), 434-453, https://doi.org/10.3301/IJG.2017.11, 2017b.
631 Brozzetti, F., Boncio, P., Cirillo, D., Ferrarini, F., de Nardis, R., Testa, A., Liberi, F., and Lavecchia, G.: High
632 resolution field mapping and analysis of the August–October 2016 coseismic surface faulting (Central Italy
633 Earthquakes): slip distribution, parameterization and comparison with global earthquakes, Tectonics, 38, 417–439,
634 https://doi.org/10.1029/2018TC005305, 2019.
635 Brozzetti, F., Mondini, A.C., Pauselli, C., Mancinelli, P., Cirillo, D., Guzzetti, F., and Lavecchia, G.: Mainshock
636 anticipated by intra-sequence ground deformations: Insights from multiscale field and SAR interferometric
637 measurements, Geosciences (Switzerland), 10(5), 186, https://doi.org/10.3390/geosciences10050186, 2020.
638 Bubeck, A., Wilkinson, M., Roberts, G.P., Cowie, P. A., McCaffrey, K.J.W., Phillips, R., and Sammonds, P.: The
639 tectonic geomorphology of bedrock scarps on active normal faults in the Italian Apennines mapped using combined
640 ground penetrating radar and terrestrial laser scanning, Geomorphology, 237, 38-51,
641 https://doi.org/10.1016/j.geomorph.2014.03.011, 2015.
642 Busby, J.P., and Merritt, J.W.: Quaternary deformation mapping with ground penetrating radar, J. appl. Geophys.,
643 41(1), 75–91, https://doi.org/10.1016/S0926-9851(98)00050-.0, 1999.
644 Cai, J., McMechan, G.A., and Fisher, M.A.: Application of ground penetrating radar to investigation of near-surface
645 fault properties in the San Francisco Bay region, Bull. seism. Soc. Am., 86(5), 1459-1470, Available online: (accessed
646 09 feb 2021), https://citeseerx.ist.psu.edu/viewdoc/download?doi=10.1.1.944.4417&rep=rep1&type=pdf, 1996.
647 Calamita, F., Pizzi, A., and Roscioni, M.: I fasci di faglie recenti ed attive di M. Vettore - M. Bove e di M. Castello -
648 M. Cardosa (Appennino Umbro-Marchigiano), In Studi Geologici Camerti; Università di Camerino: Camerino, Italy,
649 1992; 81-95, Available online: http://193.204.8.201:8080/jspui/handle/1336/552 (accessed on 09 Feb 2021), 1992.
650 Carpentier, S.F.A., Green, A.G., Langridge, R., Boschetti, S., Doetsch, J., Abacherli, A.N., Horstmeyer, H., and
651 Finnemore, M.: Flower ¨structures and Riedel shears at a step over zone along the Alpine Fault (New Zealand) inferred

https://doi.org/10.5194/se-2021-75
Preprint. Discussion started: 14 June 2021

652 from 2-D and 3-D GPR images, Journal Geophysical Research, 117(B2), B02406,
653 https://doi.org/10.1029/2011JB008749, 2012a.
654 Carpentier, S.F.A., Green, A.G., Doetsch, J., Dorn, C., Kaiser, A.E., Campbell, F., Horstmeyer, H., and Finnemore,
655 M.: Recent deformation of Quaternary sediments as inferred from GPR images and shallow P-wave velocity
656 tomograms: Northwest Canterbury Plains, New Zealand, J. Appl. Geophys., 8, 2-15,
657 https://doi.org/10.1016/j.jappgeo.2011.09.007, 2012b.
658 Cello, G., Deiana, G., Ferelli, L., Marchegiani, L., Maschio, L., Mazzoli, S., Michetti, A., Serva, L., Tondi, E., and
659 Vittori, T.: Geological constraints for earthquake faulting studies in the Colfiorito area (Central Italy), J. Seismol., 4,
660 357-364, https://doi.org/10.1023/A:1026525302837, 2000.
661 Cello G., E. Tondi, L. Micarelli, and L. Mattioni: Active tectonics and earthquake sources in the epicentral area of the
662 1857 Basilicata earthquake (southern Italy), Journal of Geodynamics, 36, 1–2, 37-50, https://doi.org/10.1016/S0264-
663 3707(03)00037-1, 2003.
664 Chiaraluce, L., Di Stefano, R., Tinti, E., Scognamiglio, L., Michele, M., Casarotti, E., Cattaneo, M., De Gori, P.,
665 Chiarabba, C., Monachesi, G., Lombardi, A., Valoroso, L., Latorre, D., and Marzorati, S.: The 2016 Central Italy
666 Seismic Sequence: A First Look at the Mainshocks, Aftershocks, and Source Models, Seismological Research Letters,
667 88(3), 757-771, https://doi.org/10.1785/0220160221, 2017.
668 Christie, M., Tsoflias, G.P., Stockli, D.F., and Black, R.: Assessing fault displacement and off-fault deformation in an
669 extensional tectonic setting using 3-D ground-penetrating radar imaging, J. appl. Geophys., 68(1), 9–16,
670 https://doi.org/10.1016/j.jappgeo.2008.10.013, 2009.
671 Cinti, F. R., Cucci, L., Pantosti, D., D'Addezio, G., and Meghraoui, M.: A major seismogenic fault in a 'silent area':
672 the Castrovillari fault (southern Apennines, Italy), Geophysical Journal International, 130(3), 595-605, Available
673 online: (accessed 09 Feb 2021), https://www.earth-prints.org/bitstream/2122/12031/1/text.pdf, 1997.
674 Cinti, F. R., Moro, M., Pantosti, D., Cucci, L., and D'Addezio, G.: New constraints on the seismic history of the
675 Castrovillari fault in the Pollino gap (Calabria, southern Italy), J. Seismol., 6, 199-217,
676 https://doi.org/10.1023/A:1015693127008, 2002.
677 Cinti, F.R., Pauselli, C., Livio, F., Ercoli, M., Brunori, C.A., Ferrario, F., Volpe, R., Civico, R., Pantosti, D., Pinzi, S.,
678 De Martini, P.M., Ventura, G., Alfonsi, L., Gambillara, R., and Michetti, A.M.: Integrating multidisciplinary, multi-
679 scale geological and geophysical data to image the Castrovillari fault (Northern Calabria, Italy), Geophys. J. Int., 203,
680 1847-1863, https://doi.org/10.1093/gji/ggv404, 2015.
681 Cirillo, D.: Digital Field Mapping and Drone-Aided Survey for Structural Geological Data Collection and Seismic
682 Hazard Assessment: Case of the 2016 Central Italy Earthquakes, Applied Sciences, 10,
683 5233, https://doi.org/10.3390/app10155233, 2020.
684 Cirillo, D., Totaro, C., Lavecchia, G., Orecchio, B., de Nardis, R., Presti, D., Ferrarini, F., Bello, S., and Brozzetti, F.:
685 Structural complexities and tectonic barriers controlling recent seismic activity of the Pollino area (Calabria-Lucania,
686 Southern Italy) – constraints from stress inversion and 3D fault model building, submitted to this special issue, Solid
687 Earth, 2021.
688 Civico, R., Pucci, S., Villani, F., Pizzimenti, L., De Martini, P. M., Nappi, R., and the Open EMERGEO Working
689 Group: Surface ruptures following the 30 October 2016 Mw 6.5 Norcia earthquake, central Italy, J. Maps, 14, 151-
690 160, https://doi.org/10.1080/17445647.2018.1441756, 2018.

https://doi.org/10.5194/se-2021-75
Preprint. Discussion started: 14 June 2021

691 Conyers, L.B.: Ground-penetrating Radar for Archaeological Mapping. In: Wiseman J., El-Baz F. (eds) Remote
692 Sensing in Archaeology, Interdisciplinary Contributions To Archaeology, Springer, New York, NY.
693 https://doi.org/10.1007/0-387-44455-6_13, 2006.
694 Conyers, L.B.: Ground-penetrating Radar for Geoarchaeology, Wiley-Blackwell, London, Wiley Online Library, 160
695 pp., doi:10.1002/9781118949993, 2016.
696 Daniels, D. J., Ground Penetrating Radar. Radar, Sonar and amp; Navigation, Institution of Engineering and
697 Technology, London: IEE Press, 752 pp, https://doi.org/10.1002/0471654507.eme152, 2004.
698 Davis, J.L., and Annan, A.P.: Ground penetrating radar for high resolution mapping of soil and rock stratigraphy,
699 Geophys. Prospect., 37, 531-551, 1989.
700 Demanet, F., Renardy, D., Vanneste, K., Jongmans, D., Camelbeeck, T., and Meghraoui, M.: The use of geophysical
701 prospecting for imaging active faults in the Roer Graben, Belgium, Geophysics, 66(1), 78–89,
702 https://doi.org/10.1190/1.1444925, 2001.
703 Dujardin, J. R., and Bano, M.: Topographic migration of GPR data: Examples from Chad and Mongolia, Comptes
704 Rendus Geoscience, 345, 2, 73-80, https://doi.org/10.1016/j.crte.2013.01.003, 2013.
705 Ercoli, M., Pauselli, C., Frigeri, A., Forte, E., and Federico, C.: "Geophysical paleoseismology" through high
706 resolution GPR data: A case of shallow faulting imaging in Central Italy, Journal of Applied Geophysics, 90, 27-40,
707 https://doi.org/10.1016/j.jappgeo.2012.12.001, 2013a.
708 Ercoli, M., Pauselli, C., Forte, E., Frigeri, A., and Federico, C.: The Mt. Pollino Fault (southern Apennines, Italy):
709 GPR signature of Holocenic earthquakes in "silent" area, in: 7th Int. Work. Adv. Gr. Penetrating Radar, IEEE, 1–6,
710 https://doi.org/10.1109/IWAGPR.2013.6601510, 2013b.
711 Ercoli, M., Pauselli, C., Frigeri, A., Forte, E., and Federico, C.: 3-D GPR data analysis for high-resolution imaging of
712 shallow subsurface faults: The Mt Vettore case study (Central Apennines, Italy), Geoph. J. Int., 198(1), 609-621,
713 https://doi.org/10.1093/gji/ggu156, 2014.
714 Ercoli, M., Pauselli, C., Cinti, F.R., Forte, E., and Volpe, R.: Imaging of an active fault: Comparison between 3D GPR
715 data and outcrops at the Castrovillari fault, Calabria, Italy, Interpretation, 3(3), SY57-SY66,
716 https://doi.org/10.1190/INT-2014-0234.1, 2015.
717 Ercoli, M., Di Matteo, L., Pauselli, C., Mancinelli, P., Frapiccini, S., Talegalli, L., and Cannata, A.: Integrated GPR
718 and laboratory water content measures of sandy soils: From laboratory to field scale, Construction and Building
719 Materials, 159,734-744, https://doi.org/10.1016/j.conbuildmat.2017.11.082, 2018.
720 Ercoli, M., Forte, E., Porreca, M., Carbonell, R., Pauselli, C., Minelli, G., and Barchi, M. R.: Using seismic attributes
721 in seismotectonic research: an application to the Norcia Mw = 6.5 earthquake (30 October 2016) in central Italy, Solid
722 Earth, 11, 329-348, https://doi.org/10.5194/se-11-329-2020, 2020.
723 Filice, F., Liberi, F., Cirillo, D., Pandolfi, L., Marroni, M., and Piluso E.: Geology map of the central area of Catena
724 Costiera: insights into the tectono-metamorphic evolution of the Alpine belt in Northern Calabria, Journal of Maps,
725 11(1), 114-125, https://doi.org/10.1080/17445647.2014.944877, 2015.
726 Filice, F., and Seeber, L.: The Culmination of an Oblique Time-Transgressive Arc Continent Collision: The Pollino
727 Massif Between Calabria and the Southern Apennines, Italy, Tectonics, 38(1), 3261-3280,
728 https://doi.org/10.1029/2017TC004932, 2019.
729 Forte, E., and Pipan, M.: Review of multi-offset GPR applications: Data acquisition, processing and analysis, Signal
730 Processing, 132, 210-220, https://doi.org/10.1016/j.sigpro.2016.04.011, 2017.

https://doi.org/10.5194/se-2021-75
Preprint. Discussion started: 14 June 2021

731 Frigeri, A., and Ercoli, M.: The ScanMars Subsurface Radar Sounding Experiment on AMADEE-18, Astrobiology,
732 20(11), 1338-1352, https://doi.org/10.1089/ast.2019.2037, 2020.
733 Gafarov, K., Ercoli, M., Cirillo, D., Pauselli, C., and Brozzetti, F.: Extending surface geology data through GPR
734 prospections: Quaternary faulting signature from the Campotenese area (Calabria-Italy), 2018 17th International
735 Conference on Ground Penetrating Radar (GPR), Rapperswil, pp. 1-4, doi: 10.1109/ICGPR.2018.8441611, 2018.
736 Galadini, F., and Galli, P.: Paleoseismology of silent faults in the Central Apennines (Italy): the Mt. Vettore and Laga
737 Mts. Faults, Annals of Geophysics, 46(5), 815-836, https://doi.org/10.4401/ag-3457, 2003.
738 Galli, P., and Bosi, V.: Catastrophic 1638 earthquakes in Calabria (southern Italy): New insights from
739 paleoseismological investigation. J. Geophys. Res., 108, B12004, https://doi.org/10.1029/2001JB001713, 2003.
740 Galli, P., Galadini, F., and Pantosti, D: Twenty years of paleoseismology in Italy, Earth-Science Reviews, 88(1-2),
741 89-117, https://doi.org/10.1016/j.earscirev.2008.01.001, 2008.
742 Galli, P., Galderisi, A., Peronace, E., Giaccio, B., Hajdas, I., Messina, P., Pileggi, D., and Polpletta, F.: The awakening
743 of the dormant Mount Vettore fault (2016 central Italy earthquake, Mw 6.6): Paleoseismic clues on its millennial
744 silences, Tectonics, 38, 687-705, https://doi.org/10.1029/2018TC005326, 2019.
745 Galli, P.: Recurrence times of central-southern Apennine faults (Italy): Hints from paleoseismology, Terra Nova, 32,
746 399-407, https://doi.org/10.1111/ter.12470, 2020.
747 Geoportale Nazionale – Lidar data 1 m resolution, Ministero dell'Ambiente e della Tutela del Territorio e del Mare –
748 Creative Commons License (Cc BY-SA 3.0 IT), last access February 2018.
749 Ghisetti, F., and Vezzani, L.: Structural Map of Mt. Pollino (Southern Italy), 1:50.000 Scale, SELCA, Firenze, 1983.
750 Goodman, D., Hongo, H., Higashi, N., Inaoka, H., and Nishimura, Y.: GPR surveying over burial mounds: correcting
751 for topography and the tilt of the GPR antenna, Near Surface Geophysics, 5, 383-388, https://doi.org/10.3997/1873-
752 0604.2007020, 2007.
753 Goodman, D., and Piro S.: GPR Remote Sensing in Archaeology Springer Science & Business Media (ISBN: 978–3-
754 642-31856-6), doi: 10.1007/978-3-642-31857-3, 2013.
755 Grandjaquet, C.L., and Grandjaquet, M.J.: Geologie de la zone de Diamante-Verbicaro (Calabre), Geol. Romana 1,
756 297-312, Available online: (accessed 09 Feb 2021), http://www.dst.uniroma1.it/VolumeI, 1962.
757 Grasmueck, M.: 3-D ground-penetrating radar applied to fracture imaging in gneiss, Geophysics, 61(4), 1050-1064,
758 https://doi.org/10.1190/1.1444026, 1996.
759 Grasmueck, M., Weger, R., and Horstmeyer, H.: Full-resolution 3D GPR imaging, Geophysics, 70(1), K12-K19,
760 2005.
761 Green, A.G., Gross, R., Holliger, K., Horstmeyer, H., and Baldwin, J.: Results of 3-D georadar surveying and
762 trenching the San Andreas fault near its northern landward limit, Tectonophysics, 368, 7-23,
763 https://doi.org/10.1016/S0040-1951(03)00147-1, 2003.
764 Gross, R., Holliger, K., Green, A.G., and John, B.: 3-D ground penetrating radar applied to paleoseismology: examples
765 from the Wellington Fault, New Zealand, in Proceedings of the Eighth International Conference on Ground
766 Penetrating Radar, 4084, 478–481, eds Noon, D.A., Stickley, G.F. & Longsta, D., Zurich, Switzerland, SPIE,
767 https://doi.org/10.1117/12.383615, 2000.
768 Gross, R., Green, A.G., Holliger, K., Horstmeyer, H., and Baldwin, J.: Shallow geometry and displacements on the
769 San Andreas Fault near Point Arena based on trenching and 3-D georadar surveying, Geophysical Research Letters,
770 29(20), 34-1-34-4, https://doi.org/10.1029/2002GL015534, 2002.

https://doi.org/10.5194/se-2021-75
Preprint. Discussion started: 14 June 2021

771 Gross, R., Green, A.G., Horstmeyer, H., Holliger, K., and Baldwin, J.: 3-D georadar images of an active fault: efficient
772 data acquisition, processing and interpretation strategies, Subsurf. Sens. Technol. Appl., 4(1), 19-40,
773 https://doi.org/10.1023/A:1023059329899, 2003.
774 Gross, R., Green, A.G., Horstmeyer, H., and Begg, J.H.: Location and geometry of the Wellington Fault (New
775 Zealand) defined by detailed three-dimensional georadar data, J. geophys. Res., 109, B05401,
776 https://doi.org/10.1029/2003JB002615, 2004.
777 Guidoboni E., Ferrari G., Mariotti D., Comastri A., Tarabusi G., Sgattoni G., and Valensise G.: CFTI5Med, Catalogo
778 dei Forti Terremoti in Italia (461 a.C.-1997) e nell'area Mediterranea (760 a.C.-1500), Istituto Nazionale di Geofisica
779 e Vulcanologia (INGV), doi: https://doi.org/10.6092/ingv.it-cfti5, 2018.
780 Heincke, B., Green, A.G., van der Kruk, J., and Willenberg, H.: Semblance-based topographic migration (SBTM): A
781 method for identifying fracture zones in 3D georadar data, Near Surface Geophysics, 4(2), 79-88,
782 https://doi.org/10.3997/1873-0604.2005034, 2006.
783 Horstmeyer, H., Corboz, P., Tronicke, J., Nobes, D.C., Campbell, B.A., and Green, A.G.: High-resolution geophysical
784 surveying at the Springfield Fault, New Zealand, in Proceedings of the 11th European Meeting of Environmental and
785 Engineering Geophysics, Near Surface 2005, Palermo, Italy, 5-8 Sep. 2005, 4 pp., https://doi.org/10.3997/2214-4609-
786 pdb.13.P045, 2005.
787 Huggenberger, P.: Radar facies: recognition of facies patterns and heterogeneities within Pleistocene Rhine gravels,
788 NE Switzerland, In Braided Rivers, edited by J.L. Best and C.S. Bristow, Geol. Soc. London Spec. Publ., 75, 163-
789 176, 1993.
790 Istituto Nazionale di Geofisica e Vulcanologia - INGV (2020 February, last access), https://data.ingv.it/en/.
791 Iannace, A., D'Errico, M., and Vitale, S.: Carta Geologica dell'area compresa tra Maratea, Castrovillari e Sangineto,
792 In: Vitale, S., Iannace, A. (Eds.), Analisi Dello Strain Finito in 3D Dell'Unità Pollino-Ciagola (Confine Calabro-
793 lucano, Italia Meridionale), Studi Geologici Camerti, Nuova Serie, 2, 153-167 (ISSN: 0392-0631), 2004.
794 Iannace, A., Garcia Tortosa, F.J., and Vitale, S.: The Triassic metasedimentary successions across the boundary
795 between Southern Apennines and Calabria–Peloritani Arc (Northern Calabria, Italy), Geol. J., 40, 155–171,
796 https://doi.org/10.1002/gj.1001, 2005.
797 Iannace, A., Vitale, S., D'Errico, M., Mazzoli, S., Di Staso, A., Macaione, E., Messina, A., Reddy, S.M., Somma, R.,
798 Zamparelli, V., Zattin, M., and Bonardi, G.: The carbonate tectonic units of northern Calabria (Italy): a record of
799 Apulian palaeomargin evolution and Miocene convergence, continental crust subduction, and exhumation of HP–LT
800 rocks, J. Geol. Soc. Lond., 164, 1165-1186, https://doi.org/10.1144/0016-76492007-017, 2007.
801 Imposa, S., De Guidi, G., Grassi, S., Scudero, S., Barreca, G., Patti, G., and Boso, D.: Applying geophysical techniques
802 to investigate a segment of a creeping fault in the urban area of San Gregorio di Catania, southern flank of Mt. Etna
803 (Sicily - Italy), Journal of Applied Geophysics, 123, 153-163, https://doi.org/10.1016/j.jappgeo.2015.10.008, 2015.
804 ISIDe Working Group, Italian Seismological Instrumental and Parametric Database (ISIDe), Istituto Nazionale di
805 Geofisica e Vulcanologia (INGV), https://doi.org/10.13127/ISIDE, 2007.
806 Jewell, C.J., and Bristow, C.S.: GPR studies in the Piano di Pezza area of the Ovindoli-Pezza Fault, Central Apennines,
807 Italy: Extending palaeoseismic trench investigations with high resolution GPR profiling, Near Surface Geophysics,
808 4(3), 147-153, https://doi.org/10.3997/1873-0604.2005040, 2006.
809 Jol, H.M.: Ground Penetrating Radar: Theory and Applications, Elsevier, pp 544, ISBN: 9780444533487, 2009.
810 Kagan, Y.Y., and Jackson, D.D.: Seismic Gap Hypothesis: Ten years after, J. Geophys. Res., 96(B13), 21419-21431,
811 https://doi.org/10.1029/91JB02210, 1991.

https://doi.org/10.5194/se-2021-75
Preprint. Discussion started: 14 June 2021

812 Lehmann, F., and Green, A.G.: Topographic migration of georadar data: Implications for acquisition and processing,
813 Geophysics, 65(3), 836-848, https://doi.org/10.1190/1.1444781, 2000.
814 Leonard, M.: Earthquake fault scaling: Relating rupture length, width, average displacement, and moment release,
815 Bull. Seismol. Soc. Am., 100(5A), 1971-1988, https://doi.org/10.1785/0120090189, 2010.
816 Liberi, F., Morten, L., and Piluso, E.: Geodynamic significance of the ophiolites within the Calabrian Arc. Island Arc,
817 15, 26-43, https://doi.org/10.1111/j.1440-1738.2006.00520.x, 2006.
818 Liberty, L.M., Hemphill-Haley, M.A., and Madin, I.P.: The Portland Hills Fault: uncovering a hidden fault in Portland,
819 Oregon using high resolution geophysical methods, Tectonophysics, 368(1-4), 89-103, https://doi.org/10.1016/S0040-
820 1951(03)00152-5, 2003.
821 Liner, C.L., and Liner, J.L.: Application of GPR to a site investigation involving shallow faults, The Leading Edge,
822 16(11), 1649-1651, https://doi.org/10.1190/1.1437545, 1997.
823 Malik, J.N., Sahoo, A.K., and Shah, A.A.: Ground-penetrating radar investigation along Pinjore Garden Fault:
824 implication toward identification of shallow subsurface deformation along active fault, NW Himalaya, Curr. Sci.,
825 93(10), 1422-1427, 2007.
826 Malik, J. N., Kumar, A., Satuluri, S., Puhan, B., and Mohanty, A.: Ground-Penetrating Radar Investigations along
827 Hajipur Fault: Himalayan Frontal Thrust-Attempt to Identify Near Subsurface Displacement, NW Himalaya, India",
828 International Journal of Geophysics, Article ID 608269, 7 pp., https://doi.org/10.1155/2012/608269, 2012.
829 Maschio, L., Ferranti, L., and Burrato, P.: Active extension in Val d'Agri area, southern Apennines, Italy: Implications
830 for the geometry of the seismogenic belt, Geophys. J. Int., 162, 591–609, https://doi.org/10.1111/j.1365-
831 246X.2005.02597.x, 2005.
832 Matoš, B., Zajc, M., Kordić, B., Tomljenović, B., and Gosar, A.: Quaternary fault activity in the SW Pannonian Basin:
833 GPR surveying in the Bilogora Mt. (NE Croatia), Geological Quarterly, 61(1), 18–36, doi:
834 https://doi.org/10.7306/gq.1308, 2017.
835 McCalpin, J.P.: Paleoseismology, 2nd Edition, International Geophysics Series, 95, Elsevier Publishing, 647 pp., plus
836 additional website content at: www.elsevier.com, ISBN 978-0-12-373576-8, 2009.
837 McCann, W.R., Nishenko, S.P., Sykes, I.R., and Krause, J.: Seismic gaps and plate tectonics: seismic potential for
838 major boundaries, Pure and applied geophysics, 117, 1082–1147, 1979.
839 McClymont, A.F., Green, A.G., Villamor, P., Horstmeyer, H., Grass, C., and Nobes, D.C.: Characterization of the
840 shallow structures of active fault zones using 3-D GPR data, J. geophys. Res., 113, B10315,
841 https://doi.org/10.1029/2007JB005402, 2008.
842 McClymont, A.F., Villamor, P., and Green, A.G.: Fault displacement accumulation and slip rate variability within the
843 Taupo Rift (New Zealand) based on trench and 3-D ground-penetrating radar data, Tectonics, 28, TC4005,
844 https://doi.org/10.1029/2008TC002334, 2009.
845 McClymont, A.F., Green, A.G., Kaiser, A., Horstmeyer, H., and Langridge, R.: Shallow fault segmentation of the
846 Alpine fault zone, New Zealand revealed from 2- and 3-D GPR surveying, J. Appl. Geophys., 70(4), 343–354,
847 https://doi.org/10.1016/j.jappgeo.2009.08.003, 2010.
848 Michetti, A. M., Ferreli, L., Serva, L., and Vittori, E.: Geological evidence for strong historical earthquakes in an
849 "aseismic" region: The Pollino case (Southern Italy), Journal of Geodynamics, 24:1-4, 67-86,
850 https://doi.org/10.1016/S0264-3707(97)00018-5, 1997.

Michetti, A. M., Ferreli, L., Esposito, E., Porfido, S., Blumetti, A. M., Vittori, E., Serva, L., and Roberts, G. P.: Ground Effects during the 9 September 1998, Mw = 5.6 Lauria, Earthquake and the Seismic Potential of the seismic Pollino Region in Southern Italy, Seismological Research Letters, 71(1), 31-46, https://doi.org/10.1785/gssrl.71.1.31, 2000.

Mogi K.: Two Kinds of Seismic Gaps. In: Wyss M. (eds) Earthquake Prediction and Seismicity Patterns, Contributions to Current Research in Geophysics, Birkhäuser, Basel, https://doi.org/10.1007/978-3-0348-6430-5_4, 1979.

Napolitano, F., De Siena, L., Gervasi, A., Guerra, I., Scarpa, R., and La Rocca, M.: Scattering and absorption imaging of a highly fractured fluid-filled seismogenetic volume in a region of slow deformation, Geosci. Front., 11(3), 989-998, https://doi.org/10.1016/j.gsf.2019.09.014, 2020.

Napolitano, F., Galluzzo, D., Gervasi, A., Scarpa, R., and La Rocca, M.: Fault imaging at Mt Pollino (Italy) from relative location of microearthquakes, Geophysical Journal International, 224(1), 637-648, https://doi.org/10.1093/gji/ggaa407, 2021.

Nobes, D. C., Jol, H. M., and Duffy, B.: Geophysical imaging of disrupted coastal dune stratigraphy and possible mechanisms, Haast, South Westland, New Zealand, New Zealand Journal of Geology and Geophysics, 59:3, 426-435, doi: 10.1080/00288306.2016.1168455, 2016.

Ogniben, L.: Schema introduttivo alla geologia del confine calabro-lucano, Mem. Soc. Geol. It, 8, 453-763, 1969.

Overgaard, T. and Jakobsen, P.R.: Mapping of glaciotectonic deformation in an ice marginal environment with ground penetrating radar, Journal Applied Geophysics, 47(3-4), 191-197, https://doi.org/10.1016/S0926-9851(01)00064-7, 2001.

Passarelli, L., Hainzl, S., Cesca, S., Maccaferri, F., Mucciarelli, M., Roessler, D., Corbi, F., Dahm, T., Rivalta, E.: Aseismic transient driving the swarm-like seismic sequence in the Pollino range, Southern Italy, Geophysical Journal International, 201:3, 1553–1567, https://doi.org/10.1093/gji/ggv111, 2015.

Pantosti, D. and Valensise, G.: Faulting mechanism and complexity of the November 23, 1980, Campania-Lucania earthquake, inferred from surface observations, J. Geophys. Res., 95(B10), 15,319-15,341, https://doi.org/10.1029/JB095iB10p15319, 1990.

Pastori, M., Margheriti, L., De Gori, P., Govoni, A., Lucente, F.P., Moretti, M., Marchetti, A., Di Giovambattista, R., Anselmi, M., De Luca, P., Nardi, A., Agostinetti, N.P., Latorre, D., Piccinini, D., Passarelli, L., and Chiarabba. C.: The 2011–2014 Pollino Seismic Swarm: Complex Fault Systems Imaged by 1D Refined Location and Shear Wave Splitting Analysis at the Apennines–Calabrian Arc Boundary, Front. Earth Sci., 9:618293, doi: 10.3389/feart.2021.618293, 2021.

Patacca, E. and Scandone, P.: Geological interpretation of the CROP-04 seismic line (Southern Apennines, Italy), Boll. Soc. Geol. It. (Ital. J. Geosci.), 7, 297-315, 2007.

Pauselli, C., Federico, C., Frigeri, A., Orosei, R., Barchi, M.R., and Basile, G.: Ground Penetrating Radar investigations to study active faults in the Norcia Basin (Central Italy), J. Appl. Geophys., 72, 39-45, https://doi.org/10.1016/j.jappgeo.2010.06.009, 2010.

Pauselli, C., Ercoli, M. Volpe, R. Federico, C. Mazzocca, M., and Speziali, L.: 2D and 3D GPR images of selected fault planes (Calabro-Lucania border), Report DPC-INGV-S1 Project "Base-knowledge improvement for assessing the seismogenic potential of Italy", deliverable D18/c1.1 - (https://sites.google.com/site/ingvdpcprojects1/home, Agreement INGV-DPC 2014-2015), 49 pp., 2015.

Plafker, G. and Galloway, J. P.: Lessons Learned from the Lorna Prieta, California, Earthquake of October 17, 1989, USGS Numbered Series Circular 1045, 48 pp., https://doi.org/10.3133/cir1045, 1989.

https://doi.org/10.5194/se-2021-75
Preprint. Discussion started: 14 June 2021

Pondrelli, S.: European-Mediterranean Regional Centroid-Moment Tensors Catalog (RCMT) [Data set], Istituto Nazionale di Geofisica e Vulcanologia (INGV), https://doi.org/10.13127/rcmt/euromed, http://rcmt2.bo.ingv.it/, 2002.

Pondrelli, S., Salimbeni, S., Ekström, G., Morelli, A., Gasperini, P., and Vannucci, P.: The Italian CMT dataset from 1977 to present, Phys. Earth Plan. Int., 159, 286-303, 2006.

Porreca, M., Minelli, G., Ercoli, M., Brobia, A., Mancinelli, P., Cruciani, F., Giorgetti, C., Carboni, F., Mirabella, F., Cavinato, G., Cannata, A., Pauselli, C., and Barchi, M.R.: Seismic reflection profiles and subsurface geology of the area interested by the 2016-2017 earthquake sequence (Central Italy), in: The 2016 Central Italy Seismic Sequence: Insights, implications and lessons learned, Tectonics, 37, 1116-1137, https://doi.org/10.1002/2017TC004915, 2018.

Pousse-Beltran, L., Vassallo, R., Audemard, F., Jouanne, F., Oropeza, J., Garambois, S., and Aray, J.: Earthquake geology of the last millennium along the Boconó Fault, Venezuela, Tectonophysics, 747-748, 40-53, https://doi.org/10.1016/j.tecto.2018.09.010, 2018.

Pucci, S., De Martini, P. M., Civico, R., Villani, F., Nappi, R., Ricci, T. et al., and Pantosti, D.: Coseismic ruptures of the 24 August 2016, Mw 6.0 Amatrice earthquake (central Italy), Geophysical Research Letters, 44, 2138-2147, https://doi.org/10.1002/2016GL071859, 2017.

Quitzow, H.W.: Derdeckenbaudes Kalabrischenmassivs und seiner Randgebiete, Abh. Ges. Wiss. Göttingen, Math Phys. Kl., 13, 63-179, 1935.

Reiss, S., Reicherter, K. R., and Reuther, C. D.: Visualization and characterization of active normal faults and associated sediments by high-resolution GPR Geological Society, London, Special Publications, 211, 247-255, doi:10.1144/GSL.SP.2001.211.01.20, 2003.

Roberts, G.P., Raithatha, B., Sileo, G., Pizzi, A., Pucci, S., Walker, J.F., et al.: Shallow subsurface structure of the 2009 April 6 Mw 6.3 L'Aquila earthquake surface rupture at Paganica, investigated with ground-penetrating radar, Geophys. J. Int., 183(2), 774-790, https://doi.org/10.1111/j.1365-246X.2010.04713.x, 2010.

Rovida, A., Locati, M., Camassi, R., Lolli, B., and Gasperini, P.: The Italian earthquake catalogue CPTI15, Bulletin of Earthquake Engineering, 18, 2953-2984, https://doi.org/10.1007/s10518-020-00818-y, 2020.

Salvi, S., Cinti, F.R., Colini, L., D'Addezio, G., Doumaz, F., and Pettinelli, E., Investigation of the active Celano-L'Aquila fault system, Abruzzi (central Apennines, Italy) with combined ground-penetrating radar and palaeoseismic trenching, Geophys. J. Int., 155(3), 805-818, https://doi.org/10.1111/j.1365-246X.2003.02078.x, 2003.

Sangree, J., B. and Widmier, J. M.: Interpretation of depositional facies from seismic data, Geophysics, 44, 131-60, https://doi.org/10.1190/1.1440957, 1979.

Schiattarella, M., Torrente, M., and Russo, F.: Analisi strutturale ed osservazioni morfotettoniche nel bacino del Mercure (Confine calabro-lucano), Il Quaternaio, 7, 613-626, 1994.

Scognamiglio, L., Tinti, E., and Quintiliani, M.: Time Domain Moment Tensor (TDMT) [Data set], Istituto Nazionale di Geofisica e Vulcanologia (INGV), https://doi.org/10.13127/TDMT, http://terremoti.ingv.it/tdmt, 2006.

Servizio Geologico d'Italia: 220 Verbicaro and 221 Castrovillari Sheets of the Carta Geologica D'Italia, 1. 100.000 Scale, Rome, 1970.

Shaikh, M.A., Maurya, D.M., Mukherjee, S., Vanik, N.P., Padmalal, A., and Chamyal, L.S.: Tectonic evolution of the intra-uplift Vigodi-Gugriana-Khirasra-Netra Fault System in the seismically active Kachchh rift basin, India: Implications for the western continental margin of the Indian plate, Journal of Structural Geology, 140, 104124, https://doi.org/10.1016/j.jsg.2020.104124, 2020.

https://doi.org/10.5194/se-2021-75
Preprint. Discussion started: 14 June 2021

930 Sketsiou, P., De Siena, L., Gabrielli, S., Napolitano, F., 3-D attenuation image of fluid storage and tectonic interactions
931 across the Pollino fault network, Geophysical Journal International, 226:1, 536–547,
932 https://doi.org/10.1093/gji/ggab109
933 Slater, L. and Niemi, T.M.: Ground-penetrating radar investigation of active faults along the Dead Sea Transform and
934 implications for seismic hazards within the city of Aqaba, Jordan, Tectonophysics, 368(1-4), 33-50,
935 https://doi.org/10.1016/S0040-1951(03)00149-5, 2003.
936 Smith, D. G. and Jol, H. M.: Wasatch fault (Utah), detected and displacement characterized by ground penetrating
937 radar, Environ. Eng. Geosci., 1, 489-496, 1995.
938 Spina, V., Galli, P., Tondi, E., and Mazzoli, S.: Fault propagation in a seismic gap area (northern Calabria, Italy):
939 implications for seismic hazard, Tectonophysics, 476, 357-369, 2009.
940 Stirling, M., Goded, T., Berryman, K., and Litchfield, N.: Selection of Earthquake Scaling Relationships for Seismic-
941 Hazard Analysis, Bulletin of the Seismological Society of America, 103(6), 2993-
942 3011, https://doi.org/10.1785/0120130052, 2013.
943 Tangari, A.C., Scarciglia, F., Piluso, E., Marinangeli, L., and Pompilio, L.: Role of weathering of pillow basalt,
944 pyroclastic input and geomorphic processes on the genesis of the Monte Cerviero upland soils (Calabria, Italy), Catena,
945 171, 299-315, ISSN 0341-8162, https://doi.org/10.1016/j.catena.2018.07.015, 2018.
946 Tarquini, S., Vinci, S., Favalli, M., Doumaz, F., Fornaciai, A. and Nannipieri, L.: Release of a 10-m-resolution DEM
947 for the Italian territory: Comparison with global-coverage DEMs and anaglyph-mode exploration via the web,
948 Computers & Geosciences, 38, 168-170, https://doi.org/10.1016/j.cageo.2011.04.018, 2012.
949 Tertulliani A. and Cucci, L.: New insights on the strongest historical earthquake in the Pollino region (southern Italy),
950 Seismol. Res. Lett., 85(3), 743-751, https://doi.org/10.1785/0220130217, 2014.
951 Testa, A., Boncio, P., Di Donato, M., Mataloni, G., Brozzetti, F., and Cirillo, D.: Mapping the geology of the 2016
952 Central Italy earthquake fault (Mt. Vettore – Mt. Bove fault, Sibillini Mts.): geological details on the Cupi – Ussita
953 and Mt. Bove - Mt. Porche segments and overall pattern of coseismic surface faulting, Geological Field Trips and
954 Maps, Italian Geological Society and of the Geological Survey of Italy, 11(2.1), 1-13,
955 https://doi.org/10.3301/GFT.2019.03, 2019.
956 Tortorici, L., Monaco, C., Tansi, C., and Cocina, O.: Recent and active tectonics in the Calabrian arc (Southern Italy),
957 Tectonophysics, 243(1-2), pp. 37–55, https://doi.org/10.1016/0040-1951(94)00190-K, 1995.
958 Totaro, C., Koulakov, I., Orecchio, B., and Presti, D.: Detailed crustal structure in the area of the southern Apennines–
959 Calabrian Arc border from local earthquake tomography, J. Geodyn., 82, 87-97,
960 https://doi.org/10.1016/j.jog.2014.07.004, 2014.
961 Totaro, C., Seeber, L., Waldhauser, F., Steckler, M., Gervasi, A., Guerra, I., Orecchio, B., and Presti, D.: An intense
962 earthquake swarm in the southernmost Apennines: fault architecture from high-resolution hypocenters and focal
963 mechanisms, Bull. Seismol. Soc. Am. 105, 1-6, https://doi.org/10.1785/0120150074, 2015.
964 Tronicke, J., Villamor, P., and Green, A. G.: Detailed shallow geometry and vertical displacement estimates of the
965 Maleme Fault Zone, New Zealand, using 2D and 3D georadar, Near Surface Geophysics, 4(3), 155-161,
966 https://doi.org/10.3997/1873-0604.2005041, 2006.
967 Utzi, E. C.: Ground Penetrating Radar, Elsevier, 209 pp., http://dx.doi.org/10.1016/B978-0-08-102216-0.00001-1,
968 2017.

https://doi.org/10.5194/se-2021-75
Preprint. Discussion started: 14 June 2021

969 Wallace, S. C., Nobes, D. C., Davis, K. J., Burbank, D. W., and White, A.: Three-dimensional GPR imaging of the
970 Benmore anticline and step-over of the Ostler Fault, South Island, New Zealand, Geophysical Journal International,
971 180(2), 465-474, https://doi.org/10.1111/j.1365-246X.2009.04400.x, 2010.
972 Vanneste, K., Verbeeck, K., and Petermans, T.: Pseudo-3-D imaging of a low-slip-rate, active normal fault using
973 shallow geophysical methods: the Geleen fault in the Belgian Mass River valley, Geophysics, 73(1), B1–B9,
974 https://doi.org/10.1190/1.2816428, 2008.
975 Wells, D.L. and Coppersmith, K.J.: New empirical relationships among magnitude, rupture length, rupture width,
976 rupture area, and surface displacement, Bull. Seismol. Soc. Am., 84(4), 974-1002, 1994.
977 Wesnousky, S.G.: Displacement and geometrical characteristics of earthquake surface ruptures: Issues and
978 implications for seismic hazard analysis and the process of earthquake rupture, Bull. Seismol.Soc. Am., 98(4), 1609-
979 1632, https://doi.org/10.1785/0120070111, 2008.
980 Vezzani, L., Festa, A., and Ghisetti, F.C.: Geology and tectonic evolution of the Central-Southern Apennines, Italy,
981 Special Paper of the Geological Society of America, 469, 1-58, https://doi.org/10.1130/SPE469, 2010.
982 Villani, F. and Pierdominici, S.: Late Quaternary tectonics of the Vallo di Diano basin (southern Apennines, Italy),
983 Quat. Sci. Rev., 29, 3167-3183, https://doi.org/10.1016/j.quascirev.2010.07.003, 2010.
984 Villani, F., Pucci, S., Civico, R., De Martini,P. M., Cinti, F. R., and Pantosti, D.: Surface faulting of the 30 October
985 2016 Mw 6.5 central Italy earthquake: Detailed analysis of a complex coseismic rupture, Tectonics, 37, 3378-3410,
986 https://doi.org/10.1029/2018TC005175, 2018.
987 ~~Vittori, E., Deiana, G., Esposito, E., Ferreli, L., Marchegiani, L., Mastrolorenzo, G., Michetti, A.M., Porfido, S., Serva,~~
988 ~~L., Simonelli, A.L., and Tondi, E.: Ground effects and surface faulting in the September-October 1997 Umbria-Marche~~
989 ~~(Central Italy) seismic sequence, J. Geodyn., 29, 535-564, https://doi.org/10.1016/S0264-3707(99)00056-3, 2000.~~
990 Yalciner, C.C., Altunel, E., Bano, M., Meghraoui, M., Karabacak, V., and Akyuz, H. S.: Application of GPR to normal
991 faults in the Büyük Menderes Graben, Western Turkey, Journal of Geodynamics, 65, 218-227,
992 https://doi.org/10.1016/j.jog.2012.05.011, 2013.
993 Zajc, M., Celarc, B., and Gosar, A.: GPR Study of a Thrust-Fault in an Active Limestone Quarry (SW Slovenia),
994 JEEG, 23(4), 457-468: https://doi.org/10.2113/JEEG23.4.457, 2018.
995 Zhang, D., Li, J., Liu, S., and Wang, G.: Multi-frequencies GPR measurements for delineating the shallow subsurface
996 features of the Yushu strike slip fault, Acta Geophys., 67, 501-515, https://doi.org/10.1007/s11600-019-00271-9,
997 2019.

https://doi.org/10.5194/se-2021-75
Preprint. Discussion started: 14 June 2021

Solid Earth
Discussions
Open Access
EGU

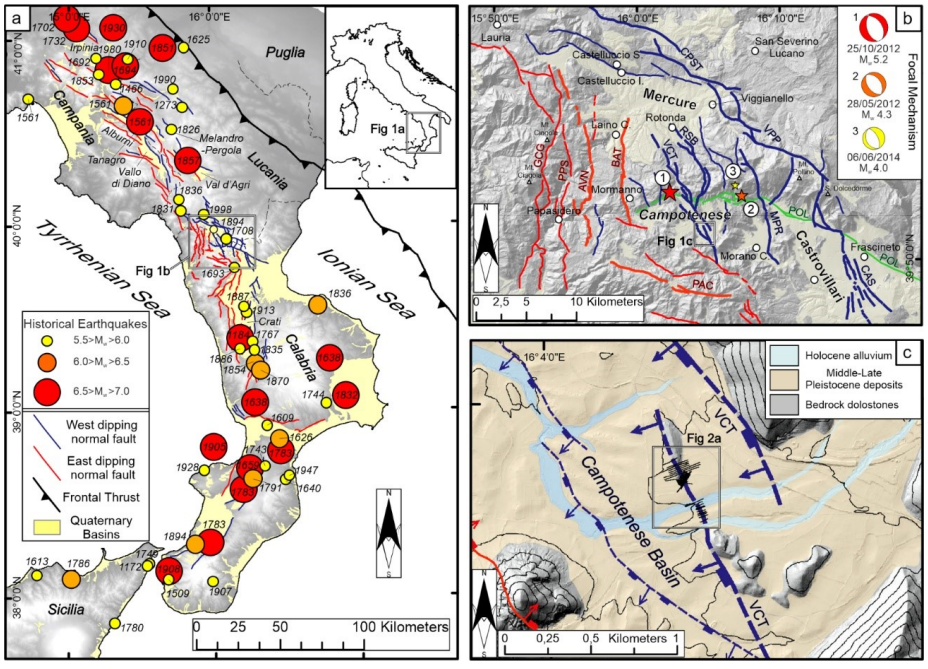

998
999

Figure 1

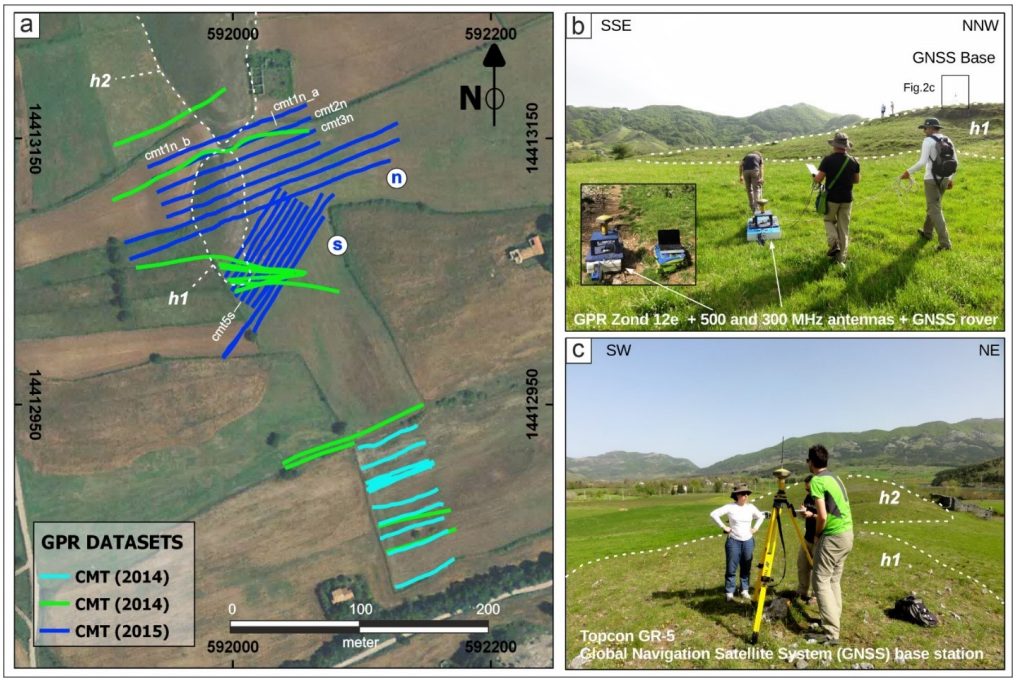

1000
1001

Figure 2

https://doi.org/10.5194/se-2021-75
Preprint. Discussion started: 14 June 2021

Solid Earth
Discussions
Open Access
EGU

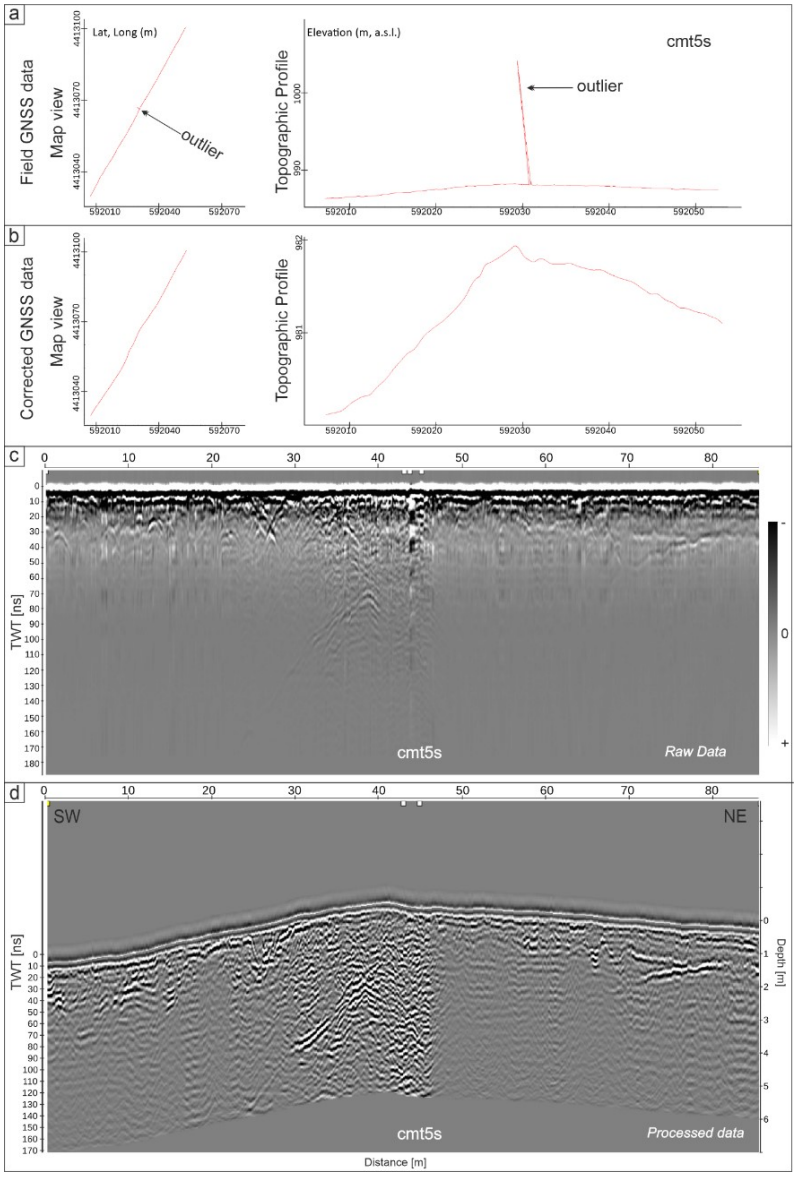

Figure 3

https://doi.org/10.5194/se-2021-75
Preprint. Discussion started: 14 June 2021

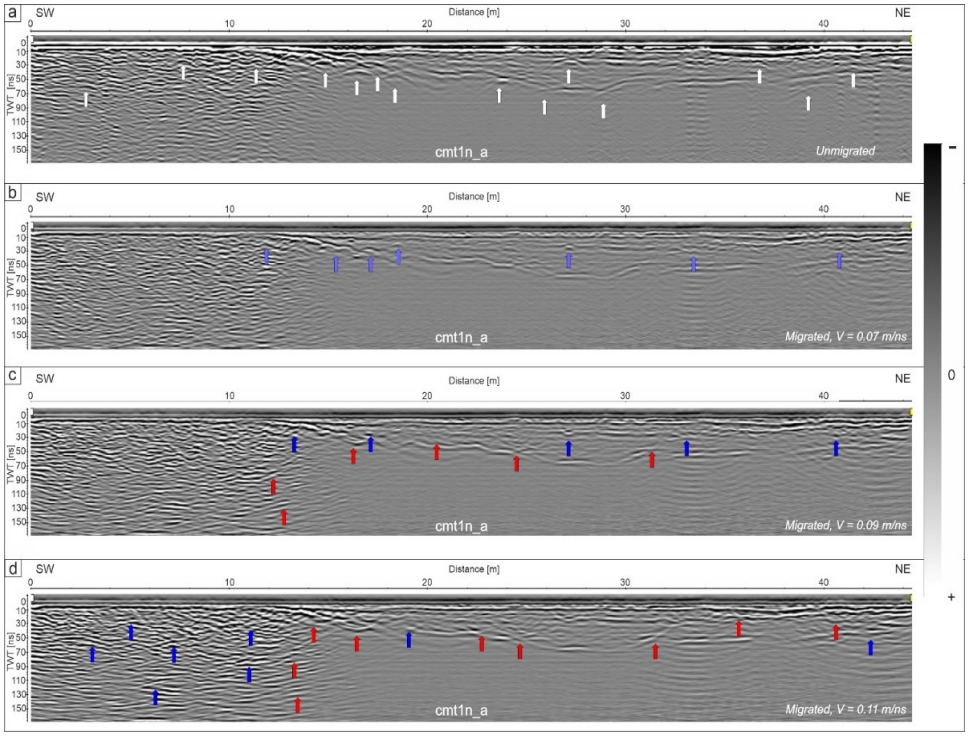

Figure 4

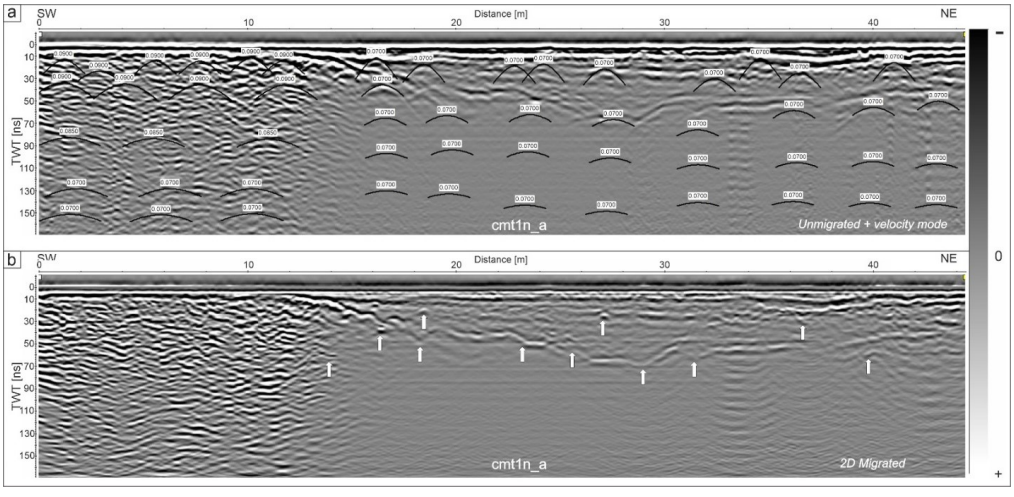

Figure 5

https://doi.org/10.5194/se-2021-75
Preprint. Discussion started: 14 June 2021

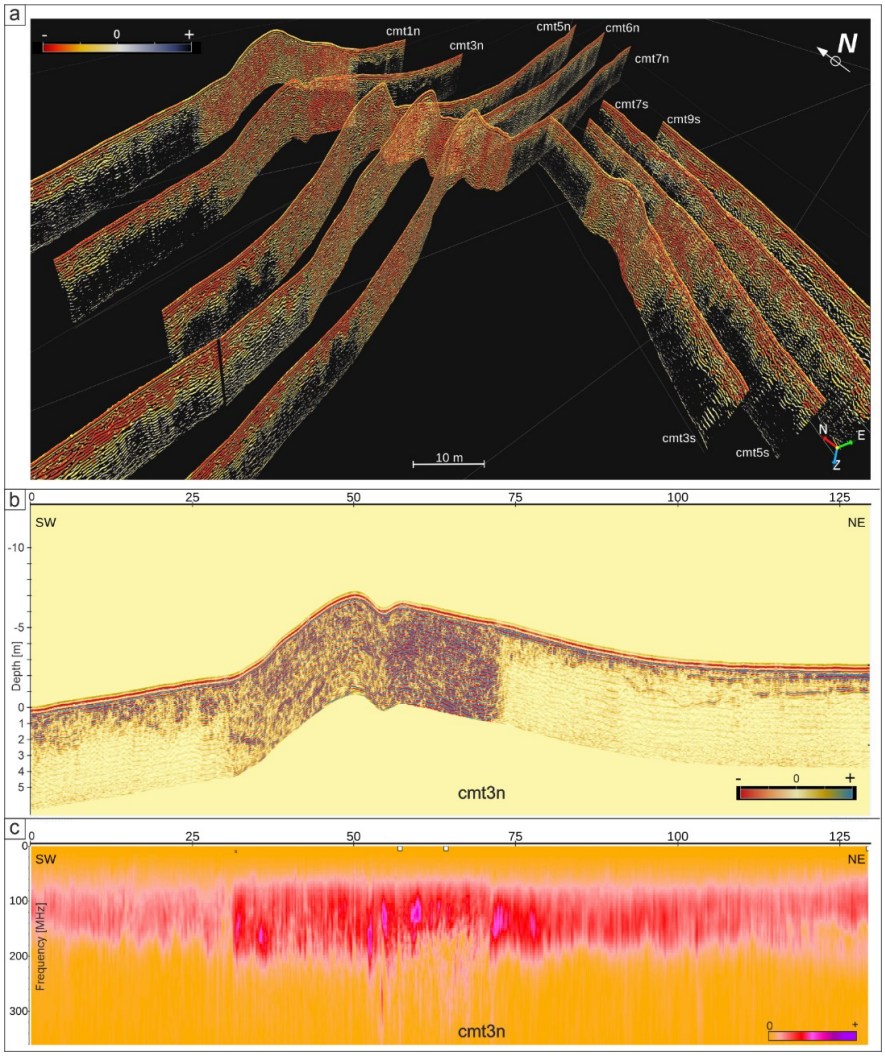

1008
1009 **Figure 6**

https://doi.org/10.5194/se-2021-75
Preprint. Discussion started: 14 June 2021

Solid Earth
Discussions
Open Access
EGU

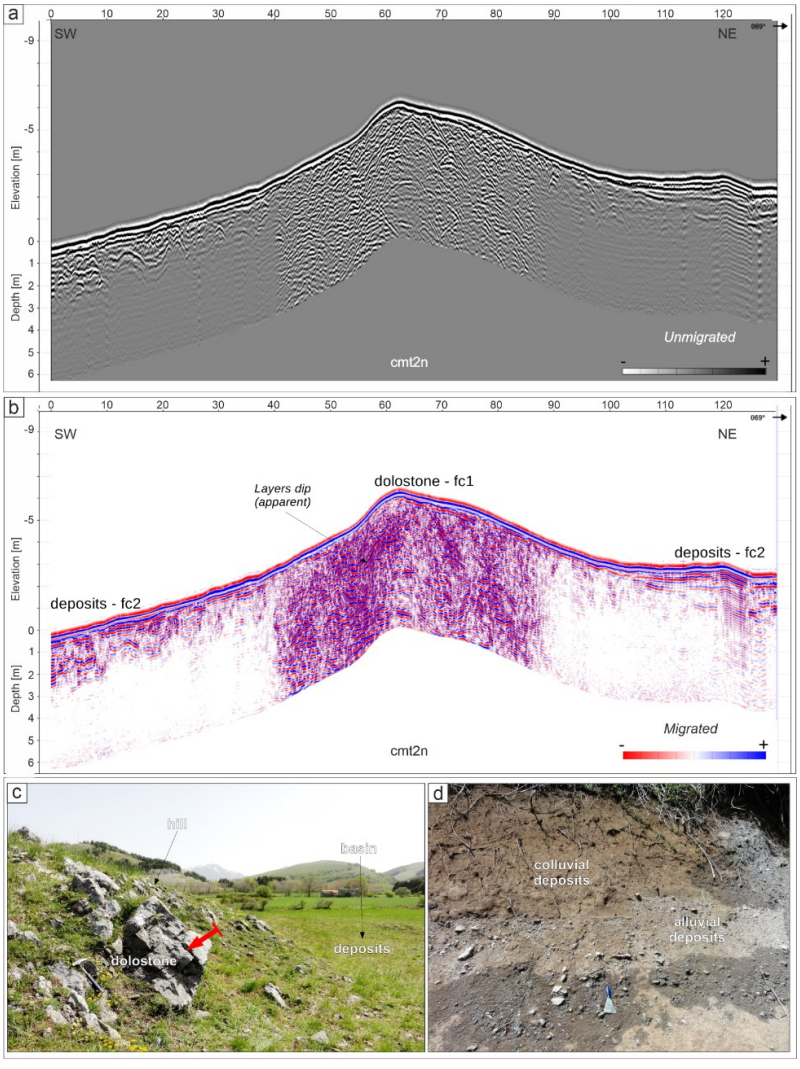

1010
1011 **Figure 7**

https://doi.org/10.5194/se-2021-75
Preprint. Discussion started: 14 June 2021

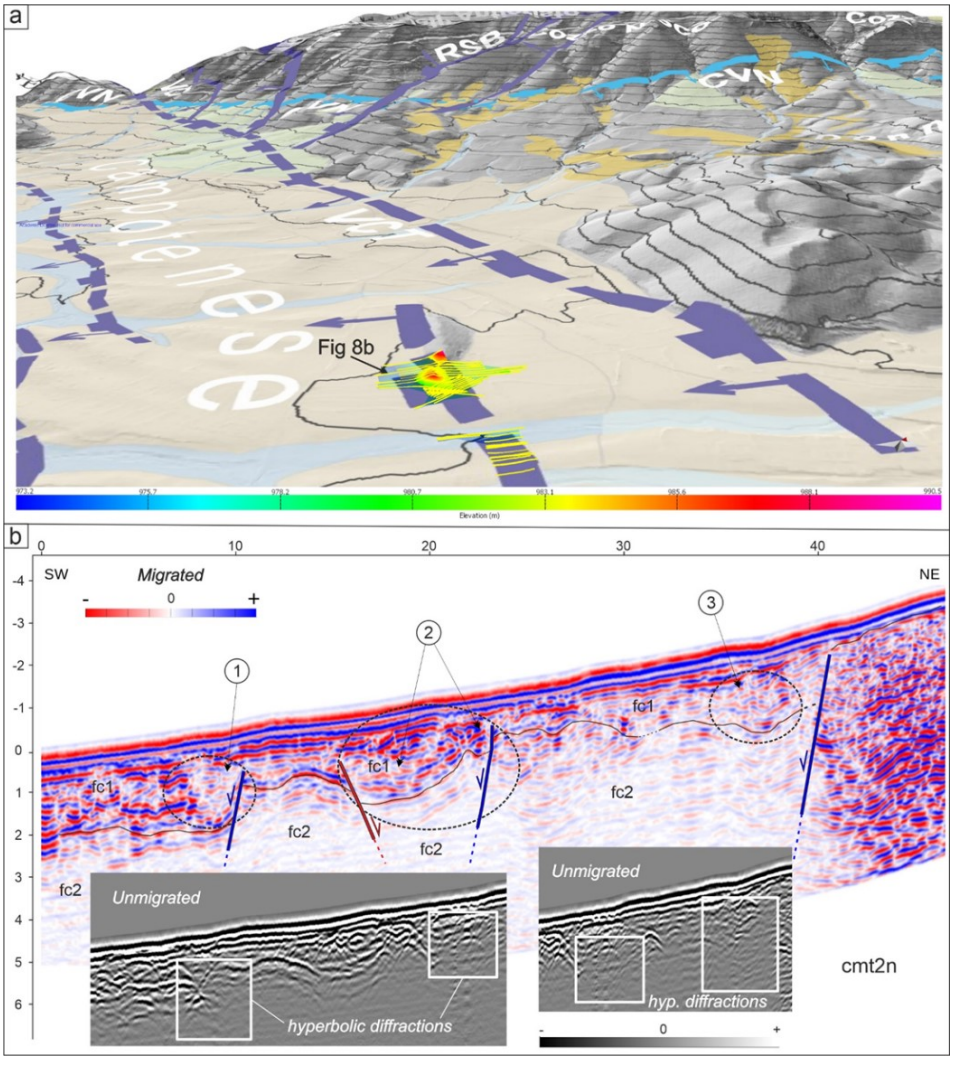

Figure 8

https://doi.org/10.5194/se-2021-75
Preprint. Discussion started: 14 June 2021

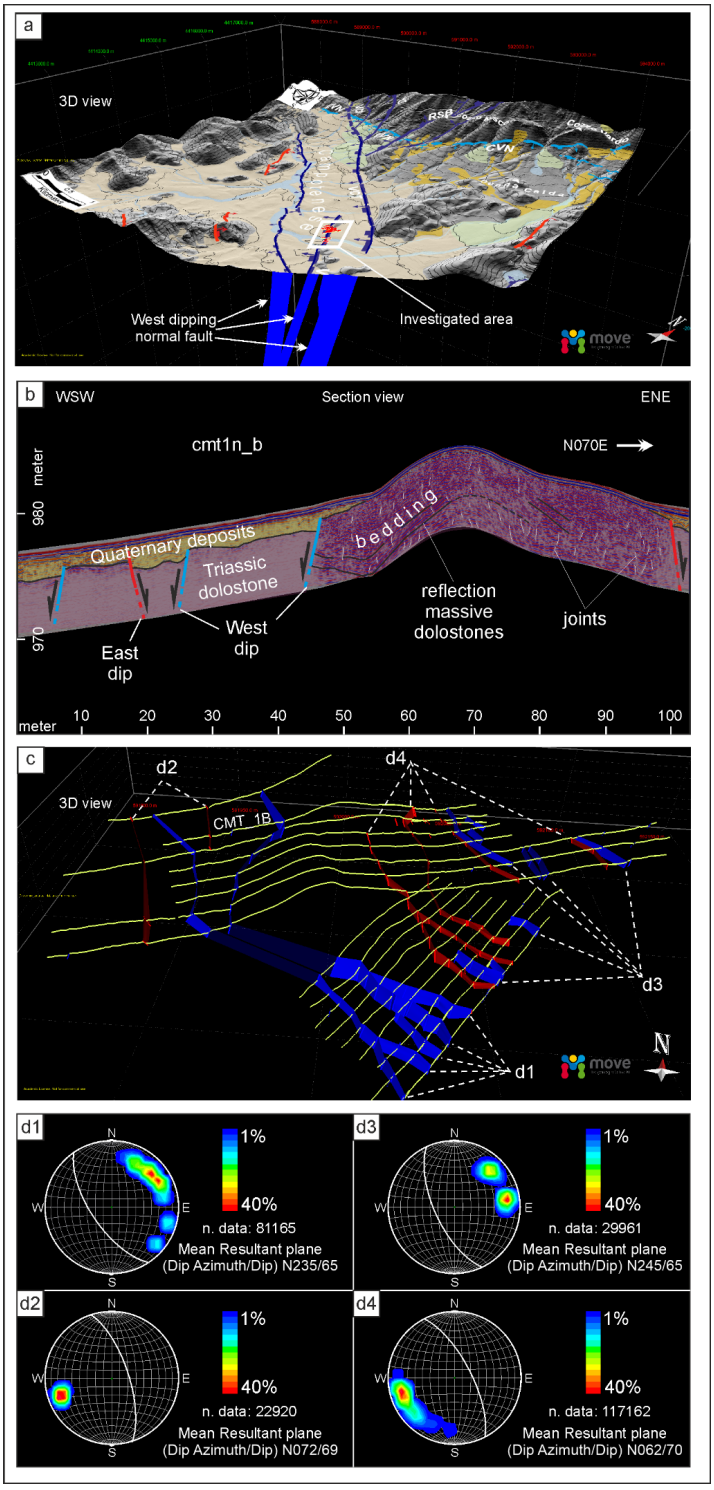

Figure 9

https://doi.org/10.5194/se-2021-75
Preprint. Discussion started: 14 June 2021

1017 **Table 1**

GPR survey information and parameters		
Antenna frequency (MHz)	300 (preferred)	500
Number of acquired profiles	45	4
Total profile length (m)	3789.5/4153	363.5/4153
Profile distance (m)	10 and 25 (in g1 and g2)	not regular
Traces distance (m)	0.05	0.02
Number of samples	1024	512
Time window (ns)	300-200*	200-100*

1018 **Table 2**

Processing Flow	**Parameters (300 MHz)**	**Parameters (500 MHz)**
Trace editing, coordinates editing and corrections	-	-
Time-zero correction	-	-
Dewow (ns)	10	5
Amplitude recovery function: $g(t)=(1+a*t)*e^{(b*t)}$	linear: 0.5 (2014) & 1.2 (2015) exponent: 0.15 (2014) & 0.6 (2015)	linear: 0.5 (2014) & 1.2 (2015) exponent: 0.15 (2014) & 0.6 (2015)
Velocity analysis	Diffraction hyperbola fittying	Diffraction yperbola fitting
Background removal (ns)	Applied from 5 ns to end (computed on all the traces)	Applied from 5 ns to end (computed on all the traces)
Bandpass filter (MHz)	32/96/650/700	64/112/750/800
F-K filter	customized	customized
Time migration (2D Kirchhoff)	2D velocity models	2D velocity models
Topographic correction	GNSS/GIS Elevations	GNSS/GIS Elevations
Time-depth conversion (Quaternary deposits)	v = 0,7 m/ns	v = 0,7 m/ns

1019
1020

1021 ## Figures and Tables captions:

1022 **Figure 1 - Location maps of the study site (DTM sources: TINITALY by Tarquini et al., 2012 and by Regione**
1023 **Calabria - www.regione.calabria.it, under license IODL 2.0. - https://www.dati.gov.it/iodl/2.0/): a) the image**
1024 **illustrates the southern Italian peninsula with the regional faults pattern and the historical strong earthquakes;**
1025 **b) map showing the studied region with local faults, and ~~the detailed location of the three historical seismic~~**
1026 **~~events~~ (stars); c) ~~detailed~~ location of the GPR survey area within the Campotenese Quaternary basin crossing**
1027 **a possible VCT fault splay.**

https://doi.org/10.5194/se-2021-75
Preprint. Discussion started: 14 June 2021

Figure 2 - GPR acquisition campaigns: a) GPR grids collected at the study site during the three field visits (aerial image source: Regione Calabria - www.regione.calabria.it, under license IODL 2.0. - https://www.dati.gov.it/iodl/2.0/); b) acquisition phase using the 300 and 500 MHz antennae (in the insert) and GNSS receiver used for accurate data positioning; c) GNSS base station set up during the fieldwork.

Figure 3: Topographic correction of GPR profiles: a) example of accuracy degradation of GNSS data, displaying an outlier both in map view and in topographic profile, on which the positioning error is considerable; b) GNSS coordinates and topographic profile after the correction; c) raw GPR section displaying high reflectivity in the central sector; d) example of full processed profile with topography displaying various reflection patterns encompassing dipping reflections and diffractions. Vertical exaggeration is 4.

Figure 4: Migration tests performed during the GPR data processing: a) unmigrated 2D GPR profile, 300 MHz antennae; b) migrated profile using a constant velocity v = 0.07 m/ns, light-blue arrows indicate good diffractions collapse; c) migration output obtained with a constant velocity v = 0.09 m/ns, with dark-blue arrows suggesting good migration results (migration artefacts are shown by red arrows); d) migration results using a constant velocity v = 0.11 m/ns, with dark-blue arrows highlighting good hyperbolas collapse, particularly within the high reflective unit; red arrows highlight clear migration smiles.

Figure 5: Example of 2D time-migration of radar profiles: a) example of hyperbolic diffractions fitting used for 2D velocity model building; a constant velocity value has been assumed in deeper no-diffraction areas for interpolation purposes; b) 2D time-migration results, highlighting the good performance of the process, which collapsed the hyperbolic diffractions and restored reliable reflection geometry.

Figure 6: GPR data visualization: a) fence diagram showing the three-dimensional location of some representative GPR profiles in the northern sector of the study site; b) bidimensional GPR profile displaying the central high reflective sector and dipping reflections across the hill; c) spatial variation of a 2D amplitude-frequency spectrum linked to variable physical properties of media along the profile. Vertical exaggeration is 4.

Figure 7: Correlation between GPR profiles and outcropping geology at the study site: a) unmigrated 300 MHz profile displaying numerous hyperbolic diffractions; b) migrated profile displaying the apparent vs true layer dip associated to fractured dolostone formation (facies fc1) and Quaternary deposits in attenuated sectors (GPR facies fc2); c) Triassic Dolostone formation outcropping on the hill (red arrow indicates the bedding) and nearby Quaternary deposits of the basin; d) an example of Quaternary colluvial and alluvial deposits outcropping nearby the survey site. Vertical exaggeration is 2.5.

Figure 8: GPR data interpretation: a) three-dimensional image of the surveyed area, displaying the Dolostone outcrops bounding the basin and the surveyed hill. The coloured surface represents the interpolated horizon reconstructed after the picking of the interpreted Dolostone top reflection (DTM source: Regione Calabria - www.regione.calabria.it, under license IODL 2.0. - https://www.dati.gov.it/iodl/2.0/); b) migrated radar profile with the main interpreted fault splays and related sedimentary structures within the Quaternary deposits (detail of unmigrated data in the two grey inserts): 1) semi-continuous and sub-horizontal reflections (fc1, Quaternary deposits) onlapping the lower boundary (Dolostone top, black line above fc2); reflections package thickening and truncation with localized attenuation, which suggest the presence of a colluvial-wedge close to a W-dip normal fault (~0.6 m vertical offset); 2) mode discontinuous, from subparallel to wavy reflections package (fc1) downlapping the lower Dolostone top boundary; the asymmetric, truncated reflectors thickening is bounded by two possible conjugate normal fault strands (~0.5 m offset) displacing both fc1 and fc2; 3) contorted reflections package with limited continuity, displaying thickening, truncation and distributed attenuation, suggesting colluvial wedge deposits lying above fc2 close to a fault zone with a W-dip normal fault (~0.8 m vertical offset). Vertical exaggeration is 2.

Figure 9: Results of the three-dimensional analysis and interpretation performed on the entire GPR dataset: a) 3D structural model inferred after the geological mapping at the scale of the basin (DTM sources: TINITALY by Tarquini et al., 2012 and by Regione Calabria - www.regione.calabria.it, under license IODL 2.0. - https://www.dati.gov.it/iodl/2.0/); b) GPR section view with interpretation including synthetic and antithetic fault splays; c) detailed structural scratch of faults obtained by the analysis and correlation across the entire GPR dataset d) synthetic stereo-net plots of the fault planes in c), reporting the mean Dip Azimuth / Dip angle extracted for the identified four main sets of discontinuities, with a Dip Azimuth ranging between N 235-245° and N 062-072° for the ~~for the~~ west-dipping and ~~E~~East-dipping normal faults, respectively. Vertical exaggeration is 2.

Table 1: Main information and GPR parameters used during the data collection (* the time window was adapted depending on the surveyed area).

Table 2: Customized flow and details of the parameters used during the processing of the GPR dataset.